

Zircon U-Pb Ages and Sr-Nd-Hf Isotopic Characteristics of the Huichizi Granitic Complex in the North Qinling Orogenic Belt and Their Geological Significance

Youwei Chen^①, Ruizhong Hu^{②*}, Xianwu Bi, Shaohua Dong, Yue Xu, Ting Zhou

State Key Laboratory of Ore Deposit Geochemistry, Chinese Academy of Sciences, Guiyang 550081, China

^①Youwei Chen: <https://orcid.org/0000-0002-2987-1235>; ^②RuiZhong Hu: <https://orcid.org/0000-0002-5075-7277>

ABSTRACT: The Huichizi granite complex is the largest Paleozoic I-type intrusion located in the North Qinling orogenic belt (NQB). In this study, we present systematic geochemical element data, zircon U-Pb ages, Lu-Hf isotopic data, and Sr-Nd isotopic data for the Huichizi granites. In terms of mineral and chemical compositions, these granites are biotite monzonitic and alkali-feldspar granites, both of which are characterized by high SiO₂ and total alkali contents and low MgO, TiO₂, and TFeO contents. These granites are weakly peraluminous (A/CNK values are 1–1.06 for biotite monzonitic granites and 1.04–1.09 for alkali-feldspar granites) and possess the geochemical characteristics of adakitic rocks, e.g., high Sr contents (319 ppm–633 ppm), Sr/Y ratios (18.5–174), and (La/Yb)_N ratios (17.6–57) and low MgO (0.04 wt.%–0.83 wt.%), Y (3.0 ppm–17.2 ppm), and heavy rare-earth element (HREE) contents. This indicates that these rocks were most likely derived from the partial melting of a thickened lower crust. In situ zircon U-Pb dating of these granites yields Early Caledonian ages (437 Ma for biotite monzonitic granites and 424 Ma for alkali-feldspar granites), indicating that the Huichizi granitic complex is the product of multi-periodic magmatism. The positive but varying zircon $\varepsilon_{\text{Hf}}(t)$ values (+0.6 to +8.5) suggest that this thickened lower crust was mainly juvenile, i.e., accreted from depleted mantle during the Neo-Mesoproterozoic Period, but involved the ancient recycled crust. Biotite monzonitic granites formed during crust thickening at the extrusion stage, whereas the alkali granites formed during crust thickening at the extension stage (post extrusion). The Huichizi granite complex witnessed the process of extrusion to extension because of the collision between the NCB and the Qinling microcontinent in the Caledonian.

KEY WORDS: U-Pb age, Sr-Nd-Hf isotope, Huichizi granitic complex, adakitic granite, North Qinling orogen.

0 INTRODUCTION

The Qinling orogenic belt (QOB) is one of the most important collision orogens in China and the most important component of the central China orogenic belt (Wu and Zheng, 2013; Zheng et al., 2012; Wu et al., 2009; Ratschbacher et al., 2003; Yang et al., 2003; Zhang G W et al., 2001, 1996; Meng and Zhang, 2000, 1999; Kröner et al., 1993; Mattauer et al., 1985). Extensive studies during the last several decades have provided new insights on the tectonic framework of the Qinling orogen (Dong and Santosh, 2016; Yu et al., 2016; Zhou et al., 2016; Dong et al., 2015, 2011a, b, c; Wang et al., 2015; Wu and Zheng, 2013; Li et al., 2007; Zhang et al., 2001; Xu B et al., 2000).

The QOB is generally acknowledged as a complex orogen between the South China Block (SCB) and the North China

Block (NCB), with a long history that can be traced back to the formation of the basement in the Archean (Fig. 1a). From north to south, the QOB can be divided into four tectonic units: the southern margin of the NCB, North Qinling orogenic belt (NQB), South Qinling orogenic belt (SQB), and northern margin of the SCB (Dong et al., 2015, 2011b; Bader et al., 2013; Zhang G W et al., 2004, 1996, 1995).

Because of the multiple complex tectonic structures of the QOB, different types of granites have widely developed since the Neoproterozoic; most of these were emplaced mainly in the Neoproterozoic, Paleozoic, and Mesozoic periods (Wang H et al., 2016, 2013, 2011; Li et al., 2015; Wang X X et al., 2015; Qin et al., 2013, 2007; Zhang C L et al., 2013, 2005, 2004; Chen, 2010; Qin, 2010; Wang T et al., 2009, 1997; Zhang Z Q et al., 2006, 1999; Sun et al., 2002; Zhang G W et al., 2001; Lu et al., 1999, 1996). Note that most Paleozoic granites developed in the NQB, which has been the subject of researches over several decades to trace back the tectonic evolution of the QOB during the Paleozoic (Wang H et al., 2016, 2013; Wang X X et al., 2013; Zhang C L et al., 2013; Dong et al., 2011b; Ratschbacher et al., 2003; Zhang G W et al., 2001; Meng and Zhang, 1999). These granites developed through subduction,

*Corresponding author: huruizhong@vip.gyig.ac.cn

© China University of Geosciences and Springer-Verlag GmbH Germany, Part of Springer Nature 2018

Manuscript received June 20, 2016.

Manuscript accepted May 1, 2017.

accretion, and collision of the Shangdan Ocean or Erlangping Back-Arc Basin. However, the precise timing, formation, scale, and processes of this tectonic event are controversial (Wang H et al., 2016, 2013; Wang X X et al., 2015; Wu and Zheng, 2013; Dong et al., 2011a, b; Wang T et al., 2009; Yan et al., 2006a, b; Lu et al., 2003; Zhang G W et al., 2001, 1996; Ren et al., 1999).

The Huichizi granite complex is the largest Paleozoic I-type intrusion located in the NQB (Fig. 1b). The petrogenesis of this complex provides a good opportunity to trace the geodynamic

evolution of the NQB during the Paleozoic. Although this granite complex has been studied widely, its geologic age, petrogenesis, and geodynamic setting are still controversial (Qin et al., 2015; Liu, 2014; Lei, 2010; Wang et al., 2009, 2000; Li et al., 2001, 2000; Zhang H F et al., 1994). In this study, we present systematic geochemical element data, zircon U-Pb ages, Lu-Hf isotopic data, and Sr-Nd isotopic data from the Huichizi complex granites to constrain the timing of formation and petrogenesis and to trace the tectonic evolution of the area.

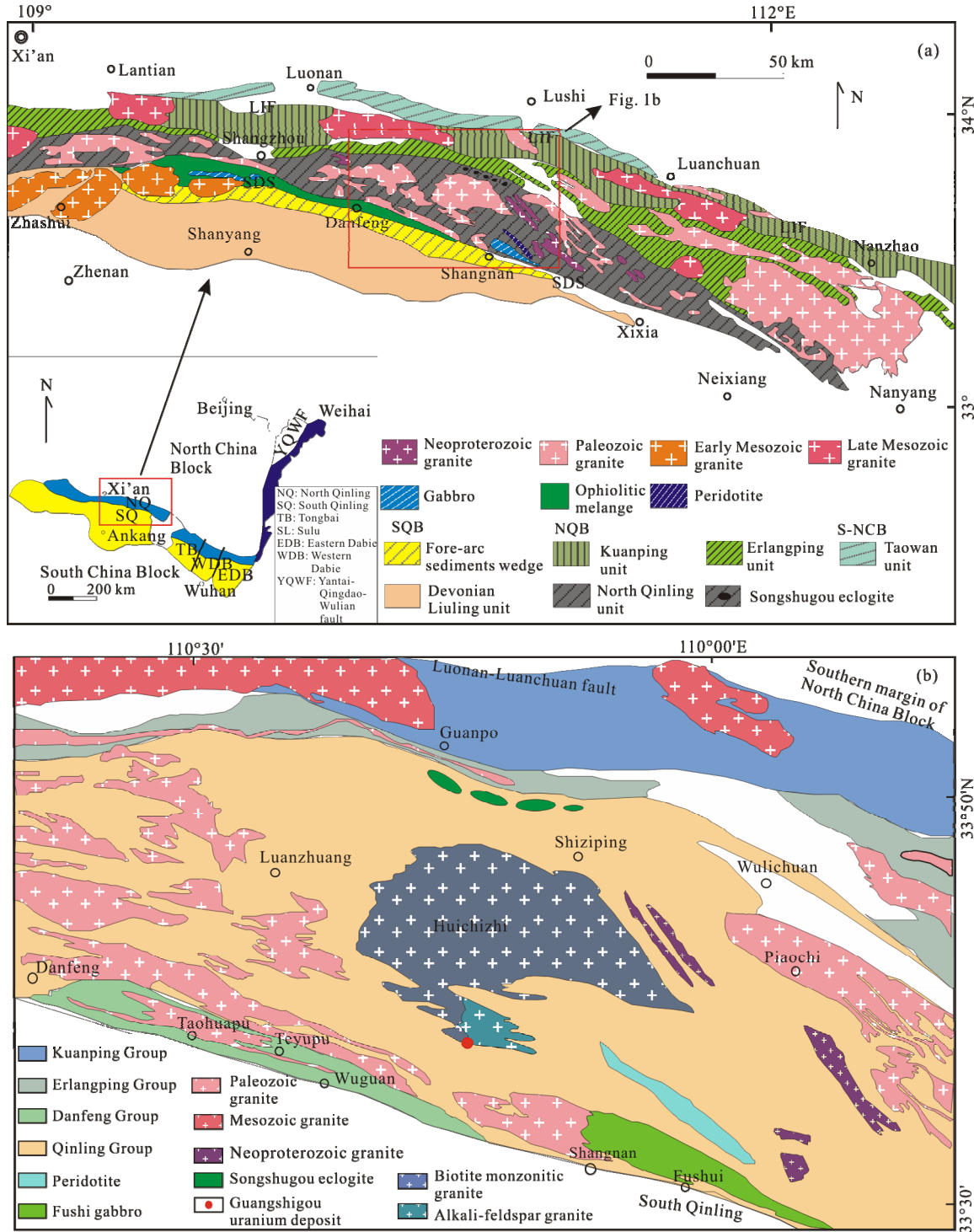


Figure 1. (a) Schematic geological map of North Qinling orogenic belt (modified after Dong et al., 2011c). (b) Geological map showing the Huichizi complex, North Qinling (modified after Zhang et al., 2013).

1 GEOLOGICAL SETTING AND SAMPLES

The NQB is bound to the north by the Luonan-Luanchuan fault and to the south by the Shangdan fault. The NQB can be traditionally subdivided from north to south into several lithological units, including the Kuanping Group, Erlangping Group, Qinling Group, Songshugou complex, and Danfeng Group, which are separated from each other by thrust faults or ductile shear zones (Fig. 1b) (Dong et al., 2015, 2011a; Wang et al., 2011; Ratschbacher et al., 2003; Zhai et al., 1998; Zhang G W et al., 1995; Zhang Z Q et al., 1994; Kröner et al., 1993).

The Kuanping Group mainly consists of metabasites (greenschist and amphibolite) and metasediments (mica schist, quartzite, and marble) (Wu and Zheng, 2013; Dong et al., 2011a; Diwu et al., 2010; Yang et al., 2003). Detrital zircons from metasedimentary rocks yielded multiphase U-Pb ages with peaks of ~2 550, ~1 750, 1 102–985, and ~650 Ma (Dong et al., 2011a; Zhu et al., 2011; Diwu et al., 2010), these data indicate that both the NQB and NCB were provenances of the continental clastic rocks of the Kuanping Group (Lu et al., 2009).

Similarly, the Erlangping Group is mainly composed of metavolcanic and metasedimentary rocks, including minor ultramafic rocks, mafic to intermediate volcanic rocks, hypabyssal dykes, clastic rocks, and cherts, which underwent upper greenschist to amphibolite facies metamorphism (Wu and Zheng, 2013; Dong et al., 2011b; Ratschbacher et al., 2003; Sun W D et al., 1996; Sun Y et al., 1996). Geochemical and geochronological data indicate that the Erlangping Group formed in an intra-oceanic arc (Wang et al., 2011; Hacker et al., 2004; Ratschbacher et al., 2003; Xue et al., 1996) or back-arc basin setting (Dong et al., 2011c; Zhang G W et al., 2004b) in the Early Paleozoic.

The Qinling Group is the most important and oldest unit of the NQB. It is composed of biotite-plagioclase and garnet-sillimanite gneisses, mica-quartz schists, graphite-bearing marbles, and amphibolites or garnet amphibolites with some eclogites (Ratschbacher et al., 2003; Zhang, 1988). Although the formation time of the Qinling Group is controversial, it is generally believed to be Paleoproterozoic (Zhang G W et al., 2001, 1995; Zhang Z W, 1994), Mesoproterozoic (Lu et al., 2006; Yang et al., 2003), and Neoproterozoic (Wan et al., 2011; Yang et al., 2010; Shi et al., 2009; Chen et al., 1991). The Qinling Group generally suffered multiphase metamorphic deformation. Reliable *in situ* Lu-Hf isochron and zircon U-Pb ages show peak metamorphic ages of 518–486 Ma (Wang et al., 2014a; Cheng et al., 2012, 2011), which are considered to be the result of the northward subduction of the Shangdan oceanic plate along the southern edge of the NQB (Liu Q et al., 2014; Dong et al., 2011c; Lei, 2010), or the result of the collision between the North Qinling microcontinent and the Erlangping oceanic arc (Wang H et al., 2014a, b, 2013, 2011).

The Songshugou complex is the largest mafic-ultramafic ophiolite complex in the NQB (Fig. 1b). Ultramafic rocks have undergone variable degrees of retrogression, whereas mafic rocks display evidence of amphibolite facies metamorphism (Cao et al., 2016; Wang et al., 2014a; Liu L et al., 2013, 2010; Lu S N et al., 2009, 2003; Chen and Liu, 2011). Both high-pressure granulites and garnet amphibolites occur as lenses within amphibolites. High-pressure granulites have metamorphic ages of 505–485 Ma (Yu et al., 2016; Chen et al., 2015;

Chen, 2004); this age was also assumed as the emplacement age of the Songshugou peridotite.

The Danfeng Group comprises a series of greenschist to amphibolite facies metavolcanic and metasedimentary rocks. Isotopic data show that the complex formed during 520–420 Ma (Dong et al., 2011a). Metavolcanic rocks exhibit the characteristics of MORB or arc-related volcanic-type rocks (Dong et al., 2011b; Yan et al., 2009; Ratschbacher et al., 2003; Zhang et al., 1995). The complex may be related to an arc-continent collision or the closure of the Shangdan Ocean Basin (Wu and Zheng, 2013; Dong et al., 2011a, b).

The Huichizi granite complex is the biggest granite batholith in the east of the NQB and covers an area of 340 km². It mainly consists of biotite monzonitic granites and sporadic outcrops of alkali-feldspar granites in the southwest (Figs. 2a, 2b). A typical pegmatite-type uranium deposit, Guangshigou Uranium Deposit, is present at the southern edges of the complex close to the granite complex, indicating a close relation with granites. We selected granites as the subject for this study. This is the first time that the relation between alkali-feldspar granites and biotite monzonitic granites has been reported for this study area.

The biotite monzonitic granite is generally gray and pale red with a medium- or coarse-grained texture (Figs. 2a, 2c). The mineral composition is mainly quartz (35%), K-feldspar (microcline) (15%–20%), plagioclase (30%–35%), and euhedral biotite (10%), with accessory hornblende, ilmenite, apatite, monazite, and zircon. The granite is characterized by gneissic schistosity, which is basically consistent with metamorphic foliation, whose direction is the same as that of the regional tectonic line. The granite has undergone some chloritization and muscovitization.

The alkali-feldspar granite appears pale red, has large mineral particles (Figs. 2b, 2d), and has a simple mineral composition primarily including quartz (35%), K-feldspar (microcline) (35%–40%), plagioclase (20%–25%), and a small amount of biotite (5%). Accessory minerals include apatite, zircon, monazite, and sphene.

Both granites intrude into the country rock of the Qinling Group, which comprises biotite plagioclase gneiss and biotite amphibolite. Migmatization is sometimes developed at the contact zone between the granites and biotite plagioclase gneiss.

2 ANALYTICAL PROCEDURES

2.1 Major and Trace Elements

Whole-rock element concentrations were analyzed at the State Key Laboratory of Ore Deposit Geochemistry, Chinese Academy of Sciences, Guiyang. Major elements were determined by X-ray fluorescence (XRF) on LiBO₄ fusion glass plates using an Axios (PW4400) XRF spectrometer. Certified standards were used for calibration. Trace elements in granites were measured by inductively coupled plasma mass spectrometry (ICP-MS; PerkinElmer, ELAN DRC-e). Relative errors were <5%. The detailed analytical procedures are given in Qi et al. (2000). Analytical errors for major and trace elements were less than 1% and 10% (relative), respectively.

2.2 Sr-Nd Isotope Analyses

For Sr-Nd isotope analyses, ~100 mg of the powdered sample was placed into a Teflon beaker with a HF/HNO₃ acid mixture.

Sr and Nd were then separated and purified by conventional cation-exchange techniques. The isotopic measurements of purified Sr-Nd solutions were performed using a Thermo Fisher thermal ionization mass spectrometer (TIMS) (Triton) at the Tianjin Institute of Geology and Mineral Resources, China Geological Survey. Mass fractionation corrections for Sr and Nd isotopes were based on $^{86}\text{Sr}/^{88}\text{Sr}=0.119\ 4$ and $^{146}\text{Nd}/^{144}\text{Nd}=0.721\ 9$, respectively.

During sample analyses, the Sr standard NBS987 yielded $^{87}\text{Sr}/^{86}\text{Sr}=0.710\ 2\pm 5$ (2σ , $n=5$) and the Nd standard LRIG yielded $^{143}\text{Nd}/^{144}\text{Nd}=0.512\ 2\pm 7$ (2σ , $n=5$). The procedural blank was 100 pg for Rb-Sr and 50 pg for Sm-Nd.

2.3 Zircon U-Pb Dating

The U-Pb dating of zircon was conducted using laser ablation (LA)-ICP-MS at the State Key Laboratory of Geological Processes and Mineral Resources, China University of Geosciences, Wuhan. Analytical conditions and data reduction were the same as those reported in Liu Y S et al. (2010, 2008). Laser sampling was performed using GeoLas 2005. An Agilent 7500a ICP-MS instrument was used for data acquisition. A blank run of 20–30 s (gas blank) was performed before the analysis of a sample for 50 s. Agilent ChemStation was used for the acquisition of each analysis. Offline selection and integration of background and analyte signals and time drift correction and quantitative calibration for trace element analyses and U-Pb dating were performed using ICPMSDataCal (Liu Y S et al., 2010, 2008). Zircon 91500 was used as an external standard for U-Pb dating and was analyzed twice for every five analyses of samples. Preferred U-Th-Pb isotope ratios used for zircon 91500 were obtained from Wieden-

beck et al. (1995), and the uncertainty in these values was propagated to sample results. Concordia diagrams were created and weighted mean calculations were performed using Isoplot/Ex (ver. 3) (Ludwig, 2003).

2.4 Zircon Lu-Hf Isotope

In situ Lu-Hf isotope analysis of zircon was performed using a New Wave UP193 LA microprobe attached to a Neptune II MC-ICP-MS at the State Key Laboratory for Mineral Deposits Research, Nanjing University. Instrumental conditions and data acquisition were similar to those described by Wu et al. (2006). A spot size of 60 μm and a repetition rate of 10 Hz were applied in all analyses. Helium was used as the carrier gas to transport an ablated sample from a LA cell to the ICP-MS torch.

To evaluate the accuracy of LA results and test the reliability of correction protocols, we repeatedly analyzed two zircon standards: 91500 and Mud Tank (MT). Our analyses yielded a mean $^{176}\text{Hf}/^{177}\text{Hf}$ ratio of $0.282\ 306\pm 0.000\ 008$ (2σ) for the 91500 zircon standard and $0.282\ 490\pm 0.000\ 004$ (2σ) for the MT zircon standard. A decay constant of $1.865\times 10^{-11}\ \text{yr}^{-1}$ was adopted for ^{176}Lu (Scherer, 2001). Initial $^{176}\text{Hf}/^{177}\text{Hf}$ ratios, denoted as $\varepsilon_{\text{Hf}}(t)$, were calculated relative to the chondritic reservoir with the present-day $^{176}\text{Hf}/^{177}\text{Hf}$ ratio of 0.282 772 and a $^{176}\text{Lu}/^{177}\text{Hf}$ ratio of 0.033 2 (Blichert and Albarède, 1997). Single-stage Hf model ages (T_{DM}) were calculated relative to the depleted mantle with a present-day $^{176}\text{Hf}/^{177}\text{Hf}$ ratio of 0.283 25 and a $^{176}\text{Lu}/^{177}\text{Hf}$ ratio of 0.038 4 (Vervoort and Blichert-Toft, 1999). Two-stage model ages (T_{DM2}) were calculated using an assumed $^{176}\text{Lu}/^{177}\text{Hf}$ ratio of 0.015 (Griffin et al., 2002).

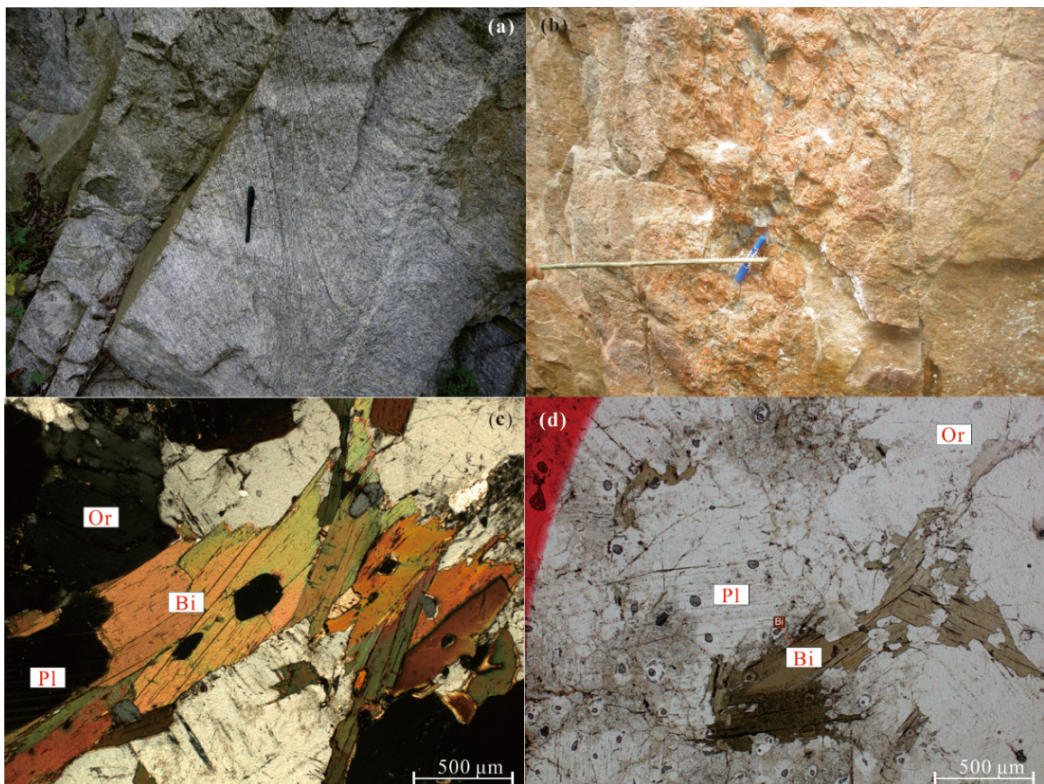


Figure 2. Field photographs showing the biotite monzonitic granite (a) and the alkali-feldspar granite (b), thin section photomicrographs of representative sample of the biotite monzonitic granite (HCZ-1) (c) and the alkali-feldspar granite (DMZ-1) (d). Bi. Biotite; Mu. muscovite; Or. orthoclase; Pl. plagioclase.

3 RESULTS

3.1 Whole-Rock Geochemistry

Table S1 presents the whole-rock chemical compositions of granites, including 14 samples from biotite monzonitic granites and seven samples from alkali-feldspar granites.

Both types of granites are characterized by high SiO_2 (69.02 wt.%–76.2 wt.%) and total alkali ($\text{Na}_2\text{O}+\text{K}_2\text{O}=7.14$ wt.%–8.74 wt.%) contents. All samples fall within the granite domain of the total alkali versus silica diagram (Fig. 3a). Biotite monzonitic granites show lower K_2O contents (1.95 wt.%–3.99 wt.%) than alkali-feldspar granites (3.69 wt.%–5.22 wt.%). This is also reflected in the $\text{K}_2\text{O}-\text{SiO}_2$ diagram (Fig. 3b). Samples from biotite monzonitic granites belong to the medium- to high-K calc-alkaline series, whereas most samples from alkali-feldspar granites fall in the high-K calc-alkaline series. Granites are weakly peraluminous ($A/\text{CNK}=1$ –1.06 for biotite monzonitic granites and $A/\text{CNK}=1.04$ –1.09 for alkali-feldspar granites; Fig. 3c) and are characterized by low MgO contents (0.04 wt.%–0.83 wt.%), TiO_2 contents of 0.03 wt.%–0.31 wt.%, and TiFeO contents of 0.21 wt.%–2.05 wt%. In Harker diagrams (Fig. 4), samples from these two plutons form two separate clusters, which show overall decreasing trends in TiO_2 , TiFeO , CaO , P_2O_5 , and Al_2O_3 , and increasing trends in SiO_2 . These results suggest fractionation by the early crystallization of mafic minerals.

The primitive mantle-normalized incompatible trace element patterns of samples from the granites are similar, with enrichment in large-ion lithophile elements (e.g., Rb, Ba, and Sr) and depletion in high-field-strength elements (e.g., Nb, Ta, P, and Ti) (Fig. 5a). They have relatively low compatible element contents (e.g., Cr and Ni). In particular, the granites exhibit high Sr contents and Sr/Y ratios and low Y and Yb contents, indicating an affinity to adakitic granites (Defant and Drummond, 1990). The chondrite-normalized patterns of representative samples (Fig. 5b) show that the granites are characterized by highly fractionated REE patterns with a steeply right-sloping chondrite-normalized pattern. The $(\text{LREE}/\text{HREE})_N$ ratios range from 15.2 to 25.7 for biotite monzonitic granites and from 10.9 to 15.97 for alkali-feldspar granites. Both granites are depleted in total REE contents ($\Sigma\text{REE}=51.2$ ppm–199.1 ppm). Biotite monzonitic granites exhibit slightly negative to strongly positive Eu anomalies ($\delta\text{Eu}=0.9$ –2.1); however, alkali-feldspar granites exhibit strongly nega-

tive Eu anomalies ($\delta\text{Eu}=0.3$ –0.5). Samples from biotite monzonitic granites exhibit an upward concave REE pattern, with more depleted MREE relative to LREE and HREE; this is suggestive of hornblende fractionation (Bottazzi et al., 1999).

3.2 U-Pb Zircon Ages

Typical magmatic oscillatory zonation is common, and few inherited cores were observed for the zircons (Fig. 6). All zircon Th/U ratios vary between 0.01 and 1.98 (average 0.28) and most clusters vary around 0.4–0.8, which is consistent with a magmatic origin (Belousova et al., 2002; Hoskin and Black, 2000). Thus, except in case of inherited cores, the ages of zircons represent the formation ages of the granites.

The entire U-Pb zircon analytical dataset is presented in Table S2 and plotted in concordia diagrams in Fig. 7. Selected zircons are mostly colorless subhedral and euhedral crystals, with the regular oscillatory zoning commonly present in magmatic zircon. Ages less than 1 000 Ma are 204-corrected $^{206}\text{Pb}/^{238}\text{U}$, whereas greater ages are 204-corrected $^{207}\text{Pb}/^{206}\text{Pb}$.

(1) Biotite monzonitic granite: Totally 33 analyses in two samples (HCZ-1 and HCZ-12) were conducted for zircon grains from two biotite monzonitic granite samples. Their U-Pb isotopic values concordantly plot in a Tera-Wasserburg diagram (Figs. 7a, 7b). Their $^{206}\text{Pb}/^{238}\text{U}$ ages range from 442 to 429 Ma (except for three zircon grains with distinct inherited cores) with weighted means of 437 ± 1.8 (MSWD=0.56) and 434 ± 2 Ma (MSWD=0.83) for the two granite samples. It is considered that these U-Pb ages can be interpreted as the crystallization age of biotite monzonitic granites. HCZ-1-4, HCZ-1-6, and HCZ-12-11 zircon grains yield ages of 916 ($^{206}\text{Pb}/^{238}\text{U}$ age), 1 466 ($^{207}\text{Pb}/^{206}\text{Pb}$ age) and 612 Ma ($^{206}\text{Pb}/^{238}\text{U}$ age) with a distinct inherited core in the CL images (Fig. 6).

(2) Alkali-feldspar granite: The plots of the alkali-feldspar granite are relatively more scattered in the Tera-Wasserburg diagram (Figs. 7c, 7d) because of the higher uranium content in the zircons compared with that of the biotite monzonitic granite. Two samples of alkali-feldspar granites have statistically identical ages. Sample DMZ-1 provided 10 concordant grains, yielding an age of 424.5 ± 2.2 Ma (MSWD=0.82). Sample DMZ-2 provided 13 concordant zircon grains, yielding an age of 426 ± 2 Ma (MSWD=0.29).

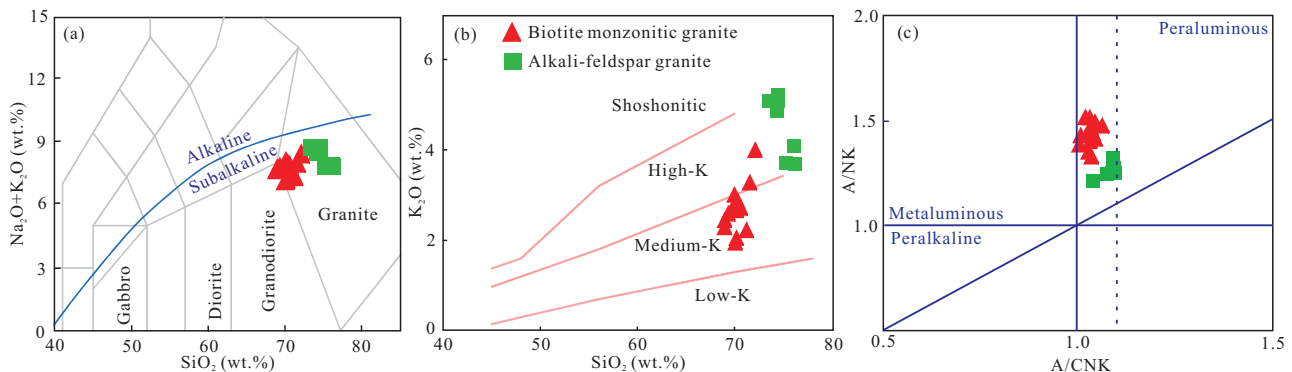


Figure 3. Plots of (a) $(\text{K}_2\text{O}+\text{Na}_2\text{O})$ vs. SiO_2 , (b) K_2O vs. SiO_2 and (c) A/NK [molar ratio $\text{Al}_2\text{O}_3/(\text{Na}_2\text{O}+\text{K}_2\text{O})$] vs. A/CNK [molar ratio $\text{Al}_2\text{O}_3/(\text{CaO}+\text{Na}_2\text{O}+\text{K}_2\text{O})$] for the biotite monzonitic granite and the alkali-feldspar granite from Huichizi complex. The $(\text{K}_2\text{O}+\text{Na}_2\text{O})$ vs. SiO_2 , (b) K_2O vs. SiO_2 diagrams are from Maniar and Piccoli (1989); The A/NK vs. A/CNK diagram are from Middlemost (1994).

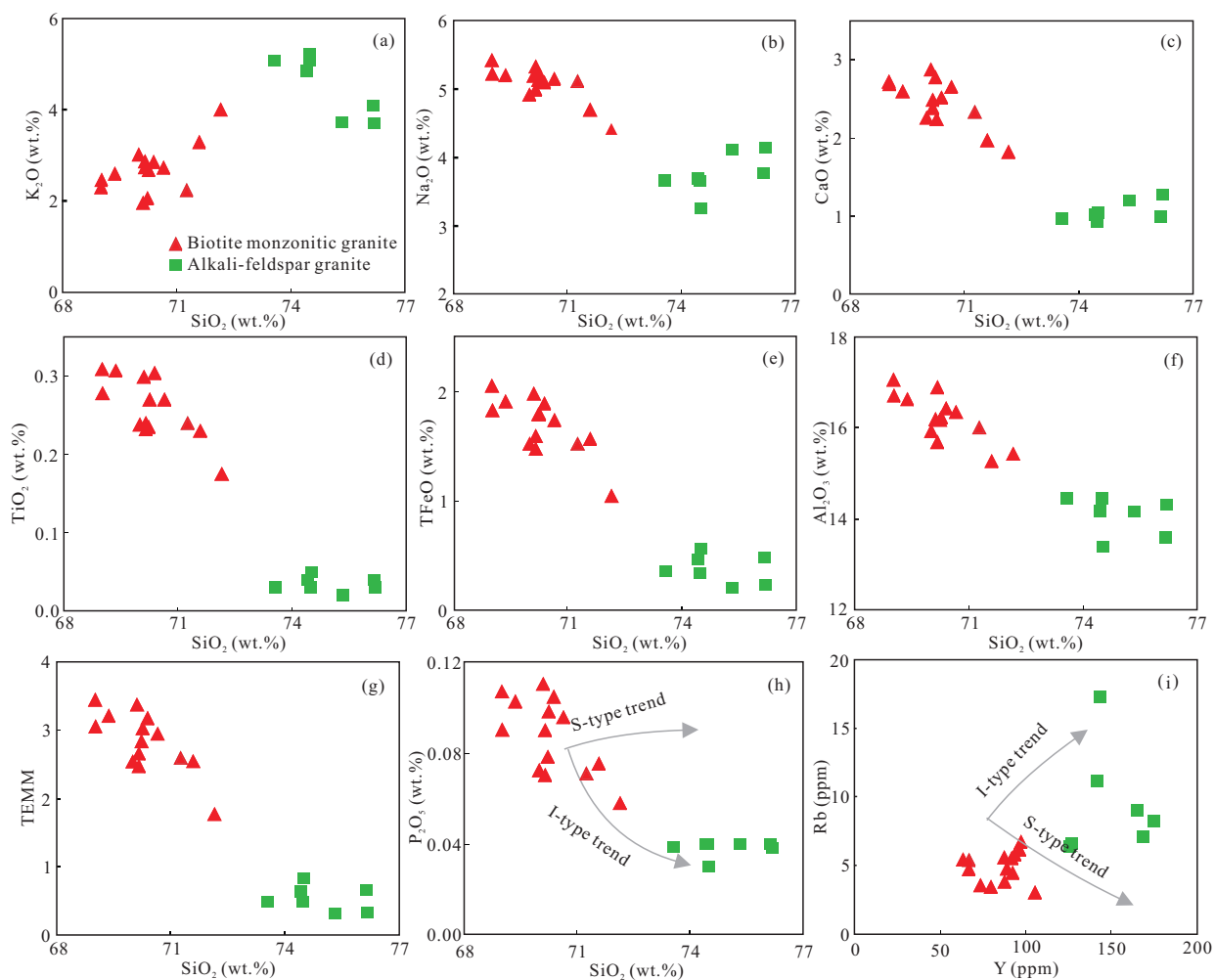


Figure 4. Major elements vs. SiO_2 (a)–(h) and Rb vs. Y (i) diagrams for the biotite monzonitic granite and the alkali-feldspar granite from Huichizi complex. (a) K_2O , (b) Na_2O , (c) CaO , (d) TiO_2 , (e) TiFeO , (f) Al_2O_3 , (g) TEMM, (h) P_2O_5 .

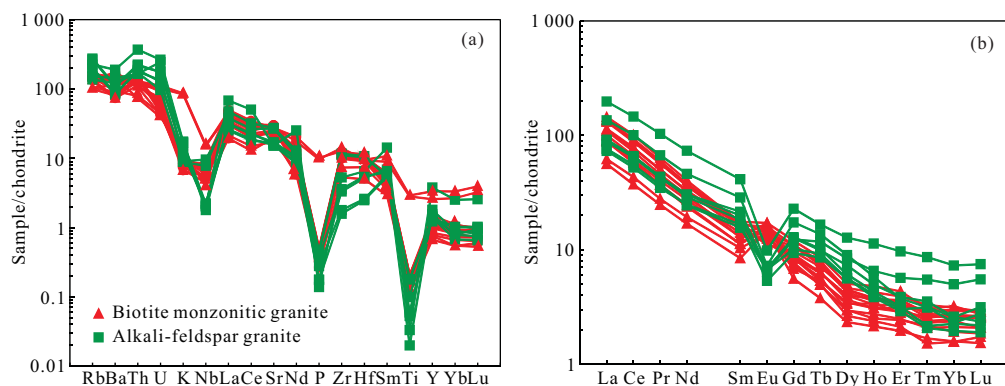


Figure 5. (a) Primitive mantle (PM) normalized trace element and (b) chondrite-normalized REE patterns diagrams for the biotite monzonitic granite and the alkali-feldspar granite from Huichizi complex. The values of chondrite and PM are from Sun and McDonough (1989).

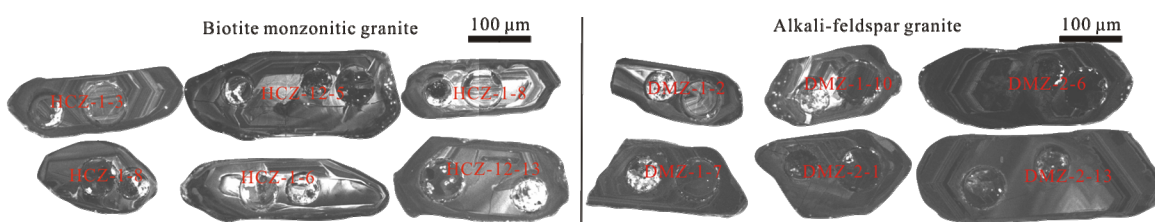


Figure 6. Representative cathodoluminescence (CL) images of zircon grains from the biotite monzonitic granite and the alkali-feldspar granite from Huichizi complex.

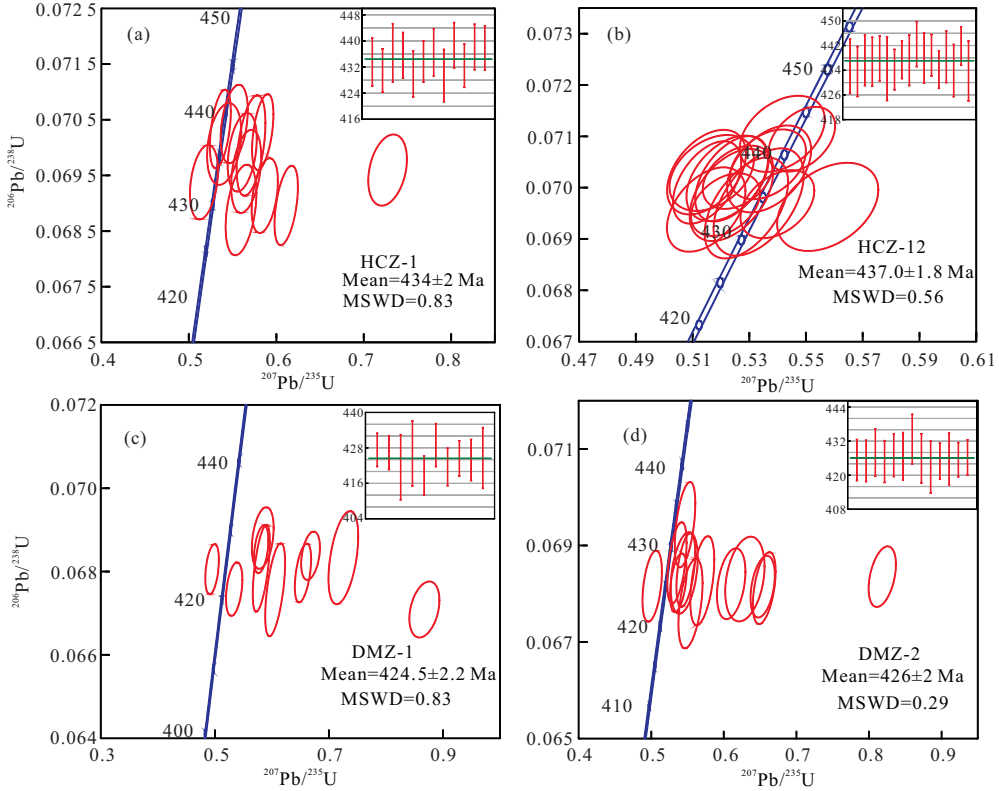


Figure 7. Zircon LA-ICP-MS concordia diagrams for the biotite monzonitic granite (a), (b) and the alkali-feldspar granite (c), (d) from Huichizi complex. The weighted mean age and MSWD are shown in each figure.

3.3 Lu-Hf Isotope Composition

The entire Lu-Hf isotope analytical dataset is presented in Table S3, $\epsilon_{\text{Hf}}(t)$ values were calculated using the weighted mean $^{206}\text{Pb}/^{238}\text{U}$ age, as determined by the U-Pb method. The $^{176}\text{Lu}/^{177}\text{Hf}$ ratios are less than 0.002 for test zircons, indicating that ^{176}Hf was rarely generated by ^{176}Lu decay and the test $^{176}\text{Lu}/^{177}\text{Hf}$ ratios can represent the Hf isotopic composition of the source (Wu et al., 2007; Amelin et al., 1999). The $f_{\text{Lu/Hf}}$ of zircons is between -0.99 and -0.94, lower than those of a mafic lower crust (-0.34; Amelin et al., 1999) and silic crust (-0.72; Vervoort and Patchett, 1996). Therefore, the Hf isotopic model age (T_{DM2}) of zircons may represent the time that the source rock separated from the mantle.

(1) Biotite monzonitic granite: Thirty-four zircon fractions from the two samples of biotite monzonitic granites were analyzed (HCZ-1 and HCZ-12). The entire analytical dataset is presented in Table S3. Zircons exhibit a wide range of $^{176}\text{Lu}/^{177}\text{Hf}$ ratios, although all values are below 0.002 1, indicating that they have low accumulation of radiogenic Hf. Three zircon fractions with distinct inherited cores show different Hf isotope compositions. The remaining 31 zircon fractions give a narrow range of initial $^{176}\text{Hf}/^{177}\text{Hf}$ of 0.282 538–0.282 748 for HCZ-1 and 0.282 630–0.282 717 for HCZ-12. These values correspond to initial $\epsilon_{\text{Hf}}(t)$ values ranging from 1 to 8.5 for HCZ-1 and 4.2 to 7.1 for HCZ-12. Each sample shows Meso to Neoproterozoic two-stage Hf model ages: 1 352 to 876 Ma for HCZ-1 and 1 151 to 963 Ma for HCZ-12.

Three zircon fractions with inherited cores were also analyzed. Zircon of HCZ-1-04 has a $^{176}\text{Hf}/^{177}\text{Hf}$ ratio of 0.282 637 ($\epsilon_{\text{Hf}}(t)=15.1$), corresponding to an age of 916 Ma. Zircon of

HCZ-1-06 has a $^{176}\text{Hf}/^{177}\text{Hf}$ ratio of 0.282 215 ($\epsilon_{\text{Hf}}(t)=11.9$), corresponding to an age of 1 466 Ma. Zircon of HCZ-12-11 has a $^{176}\text{Hf}/^{177}\text{Hf}$ ratio of 0.282 229 ($\epsilon_{\text{Hf}}(t)=-6.1$), corresponding to an age of 612 Ma.

(2) Alkali-feldspar granite: Thirty-four zircons from the two samples of alkali-feldspar granite were also analyzed. Zircons from the sample DMZ-1 exhibit varied $^{176}\text{Hf}/^{177}\text{Hf}$ ratios ranging 0.282 545–0.282 704, with $\epsilon_{\text{Hf}}(t)$ values ranging from 0.6–6.7. Sample DMZ-2 yields a narrow range of initial $^{176}\text{Hf}/^{177}\text{Hf}$ ratios, 0.282 548–0.282 752, with $\epsilon_{\text{Hf}}(t)$ values ranging from 0.9–8.2. Each sample shows Meso to Neoproterozoic two-stage Hf model ages from 1 362–892 Ma.

3.4 Sr-Nd Isotopes

Sample Rb-Sr and Sm-Nd isotope data are presented in Table S4. Initial ratios were calculated using an age of 437 Ma for biotite monzonitic granites and 424 Ma for alkali-feldspar granites.

Samples from biotite monzonitic granites exhibit a narrow range of ($^{87}\text{Sr}/^{86}\text{Sr}$)_i ratios (0.704 7–0.705 5) and positive $\epsilon_{\text{Nd}}(t)$ values (0.2–1.1). Alkali-feldspar granites are characterized by similar but more variable ($^{87}\text{Sr}/^{86}\text{Sr}$)_i ratios (0.705 7–0.706 0) and negative $\epsilon_{\text{Nd}}(t)$ values (-0.7 to -2.9).

4 DISCUSSION

4.1 Crystallized Age of the Granites

The emplacement age of the Huichizhi granites varies widely from 462 to 418 Ma (Qin et al., 2015; Liu B X, 2014; Lei, 2010; Wang et al., 2009; Li et al., 2000). These ages are acquired by the LA-ICPMS and SIMS methods, which ensure the reliability of the age data. Two ages are acquired by this

research, 434–437 Ma for the monzonitic granites and 426–424 Ma for alkali-feldspar granites. The former age is consistent with Lei (2010) and Wang et al. (2009), and the later age is consistent with Qin et al. (2015) (422±5 Ma). Taking into account the age data of Liu B X (2014), which is 462–454 Ma for the biotite granite and granodiorite, we can infer that the Huichizi complex granites are most likely produced by multiple-stage magmatism. The biotite granodiorites are intruded in 460–450 Ma; the monzonitic granites are intruded in 437–434 Ma; and the alkali-feldspar granites are intruded in 426–424 Ma.

4.2 Petrogenesis of Granites

Biotite monzonitic granites exhibit high Sr contents (366 ppm–633 ppm), Sr/Y ratios (83–174), and La_N/Yb_N ratios (26–57) and low Y (3 ppm–6.7 ppm) and Yb (0.3 ppm–0.5 ppm) contents, suggesting an affinity to adakitic granites (Defant and Drummond, 1990). Alkali granites exhibit a relatively slightly lower Sr contents (319 ppm–375 ppm), low MgO (<0.16 wt.%), Y (6.4 ppm–17.2 ppm) and Yb (0.3 ppm–1.2 ppm) contents, and high Sr/Y (19–53) and (La/Yb)_N (18–52) ratios, which also suggest an affinity to adakitic granites (Defant and Drummond,

1990). In the Sr/Y-Y and (La/Yb)_N-Yb_N diagrams (Figs. 8a, 8b), both granites plot in the adakite region. Typically, there are five possible origins for rocks with adakitic compositional features: (1) partial melting of a subducted basaltic oceanic crust (Martin, 1999; Defant and Drummond, 1990); (2) crustal assimilation and fractional crystallization (AFC) processes from parental basaltic magmas (Macpherson et al., 2006; Castillo et al., 1999; Wareham et al., 1997; Feeley and Hacker, 1995); (3) partial melting of a delaminated mafic lower crust in the mantle and subsequent interaction with mantle peridotites (Gao et al., 2004; Kay and Kay, 2002); (4) partial melting of a thickened lower crust in continental subduction/collision orogens (Chung et al., 2003; Petford and Atherton, 1996; Muir et al., 1995); and (5) a mixed origin from mantle-derived mafic magma and crust-derived felsic magma (Guo et al., 2007; Streck et al., 2007).

Adakites derived from the partial melting of a subducted young, hot, hydrated oceanic slab can be excluded because of the high silicon contents (SiO₂>65 wt.%), K₂O content (>2 wt.%), and low Na₂O. Granite rocks are not likely the product of basaltic magma AFC processes because there are no large-scale coeval basaltic and intermediate lavas related to the

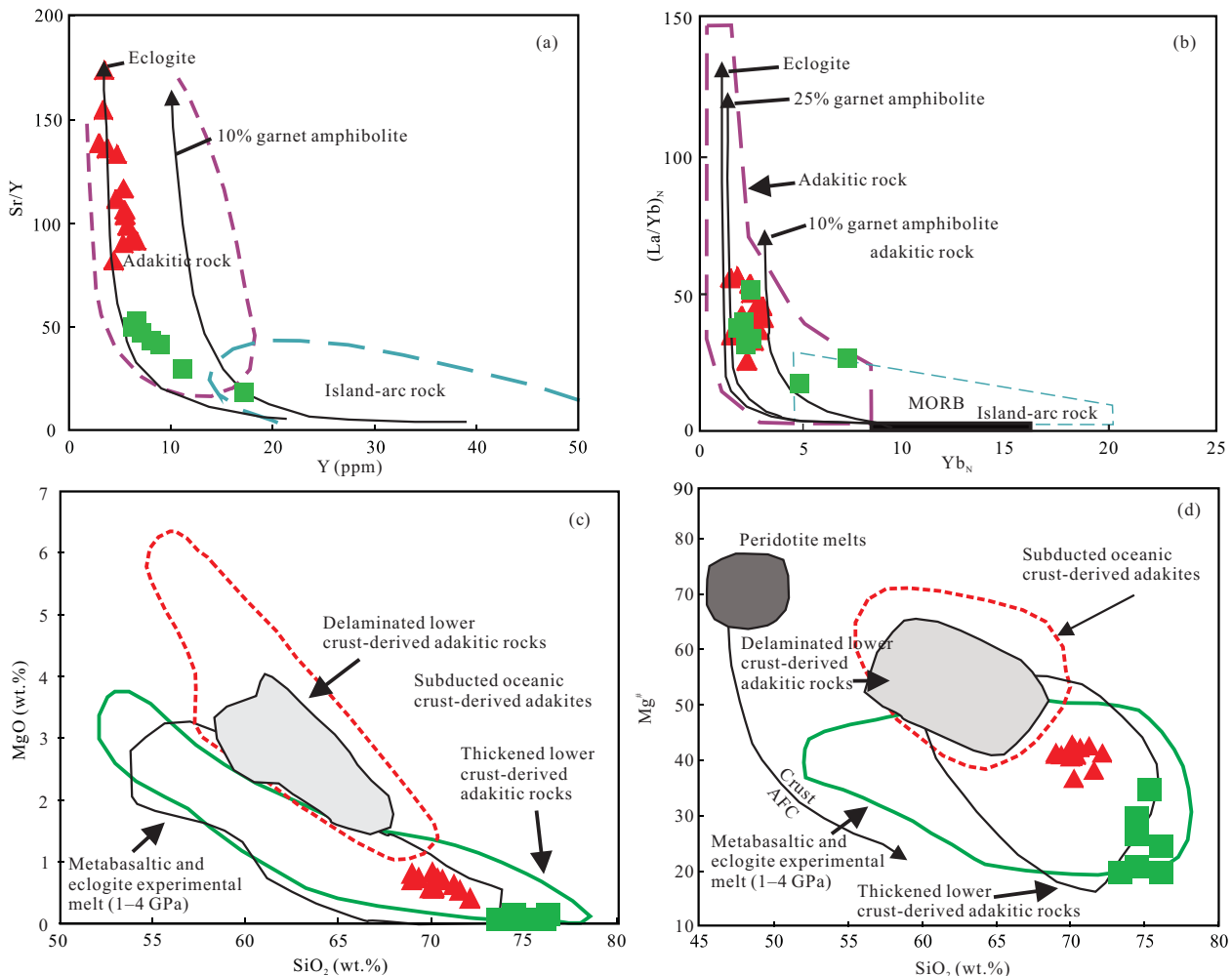


Figure 8. Diagrams of the biotite monzonitic granite and the alkali-feldspar granite from Huichizi complex. (a) Sr/Y vs. Y (Drummond and Defant, 1990), (b) (La/Yb)_N vs. Yb_N (Drummond and Defant, 1990), (c) MgO vs. SiO₂ and (d) Mg[#] vs. SiO₂ (Yu et al., 2016). The peridotite melts and crust AFC curves from Stern and Kilian (1996). The field of delaminated lower crust, subducted oceanic slab crust, and metabasaltic and eclogite experimental melts (1–4.0 GPa) follow the compilations of Huang et al. (2009) and Wang et al. (2007, 2006, 2005). Symbols are the same as in Fig. 5.

study granites. In addition, the granites show high SiO₂ contents and low K₂O contents.

The study granites could not be derived from the partial melting of the subducted basaltic oceanic crust and the delaminated lower crust. In most cases, melts derived from a delaminated thickened lower crust would also interact with the overlying mantle peridotite during magma ascent, resulting in the elevation of MgO, Mg[#], TiO₂, CaO, Na₂O, Cr, and Ni contents and relatively low SiO₂ and K₂O contents (Castillo, 2006; Wang et al., 2006; Martin et al., 2005; Prouteau et al., 2001; Smithies, 2000). These characteristics conflict with those of the study granites. A critical feature of magma-mixing models is the petrographic observation of mafic microgranular enclave and complex compositionally zoned phenocrysts, especially reversely zoned pyroxene. However, there is no such evidence in the study granites; therefore, the magma-mixing mechanism can be excluded. We consider that the partial melting of a thickened lower crust is the most likely mechanism of adakitic granite formation. In Figs. 8c and 8d, all granodiorite samples plot in the transitional field between adakitic rocks formed by the melting of a thickened lower crust and those generated by the melting of metabasaltic and eclogite experimental melts. The granites have low MgO or Mg[#] contents, which is similar to that of the experimental melts from metabasalts and eclogites (mostly Mg[#]<45, Rapp et al., 1999; Sen and Dunn, 1994). The geochemical characteristics and abovementioned results suggest that the granites were most likely derived from the partial melting of a thickened basaltic lower crust.

4.3 Source Materials

There are different views about the origin of the Huichizi complex: a mixed origin from mantle crust material (Lei, 2010; Zhang H F et al., 1994), partial melting of the mafic lower crust (Qin et al., 2015; Li et al., 2001), partial melting of the lower crustal mafic volcanic rocks (Liu B X, 2014), anatetic melting of the lower crust involving mafic material (Wang X X et al., 2015; Wang T et al., 2009).

The highly positive $\varepsilon_{\text{Hf}}(t)$ values (1–8.5 for biotite monzonitic granites and 0.6–8.2 for alkali-feldspar granites) and slightly negative to positive ε_{Nd} (0.2–1.1 for biotite monzonitic granites and -0.7 to -2.9 for alkali-feldspar granites) do not agree with the $\varepsilon_{\text{Hf}}(t)$ and ε_{Nd} values for the ancient central Qinling Group basement-derived rocks.

Meanwhile, the T_{DM2} ages of the granites are relatively young (876–1 368 Ma), indicating that the presence of an old, recycled crust in the magmatic source may be insignificant.

The positive $\varepsilon_{\text{Hf}}(t)$ values and young T_{DM2} ages of the granites indicate that the magmatic source of the granites mainly consisted of mafic material such as a subducted oceanic crust, juvenile lower crust, or upwelling mantle. As mentioned above, the major and trace element characteristics indicate that the granites are most likely related to a thickened basaltic lower crust. In addition, there is no obvious evidence of magma mixing in the study granites. Therefore, the granites were likely derived from a thickened basaltic juvenile lower crust.

The $\varepsilon_{\text{Hf}}(t)$ values of the two types of granites are similar and an individualized limited variable. Inherited zircon cores of biotite monzonitic granites provided an age of 612 Ma with a negative

$\varepsilon_{\text{Hf}}(t)$ value (-6.1). It is considered that magma source materials comprised little old recycled crust. It is concluded that the granites are mainly derived from the partial melting of a juvenile thickened basaltic lower crust and comprised little old recycled crust when melting. In addition, compared with biotite monzonitic granites, the lower $\varepsilon_{\text{Hf}}(t)$ and $\varepsilon_{\text{Nd}}(t)$ values of alkali-feldspar granites indicate that more old recycled crust was present in the granite sources. Moreover, the source materials exhibit isotopic characteristics similar to those of Songshugou mafic-ultramafic ophiolites. The $\varepsilon_{\text{Hf}}(t)$ values of the granites likely fall on the evolution trends of the Songshugou complex in the $\varepsilon_{\text{Hf}}(t)$ - t diagram (Fig. 9). This interpretation can also be confirmed by the bulk Sr-Nd isotopic compositions of the granites, whose plots fall within the field of the Songshugou complex in the $\varepsilon_{\text{Nd}}(t)$ - $(^{87}\text{Sr}/^{86}\text{Sr})_i$ diagram (Fig. 10).

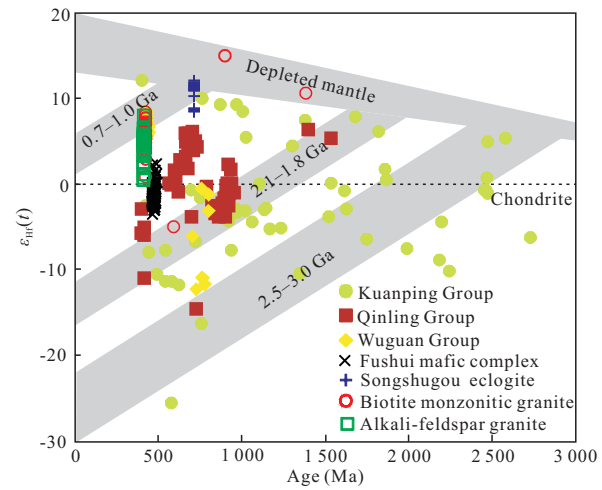


Figure 9. $^{206}\text{Pb}/^{238}\text{U}$ ages vs. $\varepsilon_{\text{Hf}}(t)$ of zircons from the biotite monzonitic granite and the alkali-feldspar granite from Huichizi complex. Data sources for the Qinling Group (Liu B X, 2014; Yan et al., 2009; Zhang Z Q et al., 1994), Kuanping Group (Zhang et al., 1995), Danfeng Group (Sun et al., 2002), Fushui complex (Liu B X, 2014; Wang et al., 2014b) and Songshugou eclogite (Qian et al., 2013; Wang X X et al., 2013).

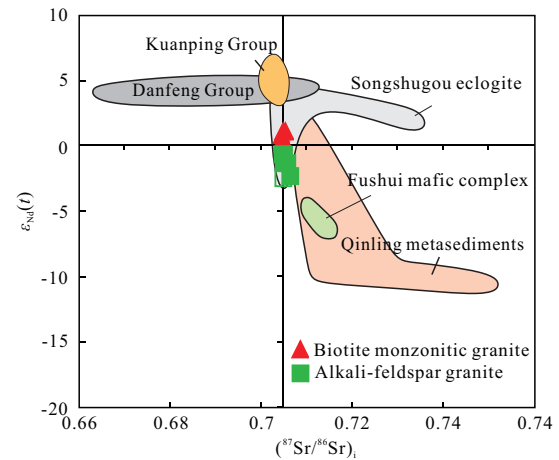


Figure 10. Initial $^{87}\text{Sr}/^{86}\text{Sr}$ vs. $\varepsilon_{\text{Nd}}(t)$ plot of the biotite monzonitic granite and the alkali-feldspar granite from Huichizi complex. Data sources for the Qinling Group (Diwu et al., 2014; Shi et al., 2013), Kuanping Group (Shi et al., 2013), Wuguan Group (Shi et al., 2013), Fushui complex (Liu, 2014; Wang et al., 2014b) and Songshugou eclogite (Wang X X et al., 2013).

In conclusion, both granites possess similar source characteristics, which are similar to those of Songshugou mafic-ultramafic ophiolites. The granites are derived from the basaltic lower continental crust accreted from the depleted mantle during the Neo-Mesoproterozoic Period. It is also indicated that continental crustal growth occurred during the Neo-Mesoproterozoic Period.

4.4 Crustal Thickness of Partial Melting

The trace element characteristics of adakitic rocks provide information to constrain residual minerals and the pressure and depth of adakitic melt generation (Zhang et al., 2015; Ma et al., 2014; Xiong et al., 2009, 2006, 2005; Xiong, 2006; Defant and Drummond, 1990). The granites were most likely derived from the partial melting of a thickened basaltic lower crust with the similar source materials, as discussed above. The REE characteristics show that both granites exhibit strong fractionation between LREE and HREE ($(\text{La/Yb})_{\text{N}}=26-57$ for biotite monzonitic granites and 18–53 for feldspar granites), high Sr contents and Sr/Y ratios, and low Yb and Y contents. These characteristics are believed to be because of the presence of garnet as the main residue phase during partial melting (Defant and Drummond, 1990). However, biotite monzonitic granites exhibit slightly negative to positive Eu anomalies, relatively higher Sr contents, and relatively lower Rb contents compared with alkali-feldspar granites, which had strongly negative Eu anomalies, indicating different residue minerals during the partial melting. It is considered that plagioclase feldspar is a minor residual mineral in biotite monzonitic granites, whereas it is more dominant in feldspar granites (Moyen, 2009; Rapp and Watson, 1995).

Nb and Ta are geochemical analogs because of their similar ionic radii and valence states (Jochum et al., 1986); therefore, the Nb/Ta ratio is barely affected during magmatic processes (Ding et al., 2013, 2009; Liang et al., 2009; Foley et al., 2002; Dostal and Chatterjee, 2000; Green, 1995). However, previous studies have revealed that rutile effectively fractionates Nb from Ta (Xiong et al., 2011; Liang et al., 2009; Foley et al., 2000). Hence, melt that is in equilibrium with residual rutile during melting will be characterized by high Nb/Ta ratios. The Nb/Ta ratios of the biotite monzonitic granites vary from 7.9 to 16.5 (average 11.5), which are higher than the average value of a lower continental crust (i.e., 8, Rudnick and Gao, 2003). This indicates the presence of rutile in the residual mineral. On the other hand, the alkali-feldspar granites are characterized by low Nb/Ta ratios, from 4 to 14.7 (average 7), which is lower than that of the lower continental crust. This phenomenon may indicate the absence of residual rutile in the magma source of alkali-feldspar granites.

It can be concluded that residual minerals during the partial melting of source for the two types of granites are quite different: more garnet and rutile but less feldspar in biotite monzonitic granites and more feldspar but less garnet and no rutile in alkali-feldspar granites. Previous studies have indicated that the stability and content of garnet and rutile will increase with the pressure increase during partial melting, accompanied by a decrease in the content of feldspar (Qian and Hermann, 2013; Xiong et al., 2011; Huang and He, 2010; Wolde and Team, 1996; Peacock et al., 1994; Sen and Dunn, 1994; Wolf and Wyllie, 1994; Beard and

Lofgren, 1991; Rapp et al., 1991; Rushmer, 1991). The experimental data on the partial melting of basic metamorphic rocks or hydrous basalt indicate that the residual mineral is eclogite when the pressure is above 2 GPa and granulite when the pressure is between 1 and 1.5 GPa (Xiong et al., 2011). The simulated calculations also indicate that feldspar is stable below a pressure of 1.5 GPa (Xiong et al., 2011, 2005; Huang and He, 2010). Therefore, we conclude that biotite monzonitic granites are derived under a pressure of above 2.0 GPa (>60 km) and alkali-feldspar granites are derived under a pressure of 1.5 GPa (<50 km).

4.5 Tectonic Implications

Multiphase metamorphic and magmatic events were developed in the NQB and accompanied by numerous igneous and metamorphic rocks, making the NQB a classic example for studying the evolution of a structure belt. Highly precise ages of high-ultrahigh pressure Paleozoic metamorphic rocks have been acquired in recent years (Chen et al., 2015; Wang et al., 2014a, 2011; Liu L et al., 2013, 2010, 2003; Chen and Liu, 2011; Liu J F et al., 2009; Yang et al., 2005, 2003, 2002). The formation and evolution of the NQB in the Paleozoic have attracted increased attention, including the development of different structure models (Dong and Santosh, 2016; Yu et al., 2016; Dong et al., 2015, 2014, 2011c; Liu et al., 2013, 2003; Shi et al., 2013; Wang X X et al., 2013; Wu and Zheng, 2013; Zhang et al., 2013; Wang T et al., 2009). It is generally known that the NQB underwent deep subduction and uplifting of the continental crust in the Paleozoic, accomplished by multiple metamorphic and magmatic events due to the evolution of the Shangdan Ocean Basin. However, there is some controversy over the origin, region, and tectonic process of the Shangdan Ocean as above mentioned.

In the Nb versus Y and Rb versus (Yb+Nb) diagrams (Fig. 11), the biotite monzonitic granite plots mainly fall in the VAG field, and the alkali-feldspar granite plots fall in the syn-COLG field, which indicate that the tectonic settings of the biotite monzonitic granite and the alkali-feldspar granite are different. Moreover, our research indicates that the granites possess adakitic characteristics, being derived from the partial melting of the thickened basaltic juvenile lower crust. The residual phases of the partial melt source of biotite monzonitic granites are mainly composed of garnet and rutile with no feldspar, which indicates a crust thickness of above 60 km when partial melting occurred. However, those of alkali granites are mainly composed of feldspar with less garnet, suggesting a crust thickness of below 50 km when partial melting occurred.

It can be concluded that the formation mechanisms of biotite monzonitic granites and alkali-feldspar granites may be related to the superimposed thickening of the lower crust due to collision between the NCB and Qinling microcontinent in the Paleozoic. Biotite monzonitic granites formed during crust thickening at the extrusion stage, whereas alkali granites formed during crust thickening at the extension stage (after the extrusion stage).

The U-Pb chronologies of zircons indicate that the granites intruded at 437 and 424 Ma. These ages are consistent with two intense Paleozoic metamorphic and magmatic activities in the NQB at ~450 and ~420 Ma (Wang X X et al., 2015; Dong et al., 2011c; Wang T et al., 2009; Zhang Z Q et al., 2006; Hu

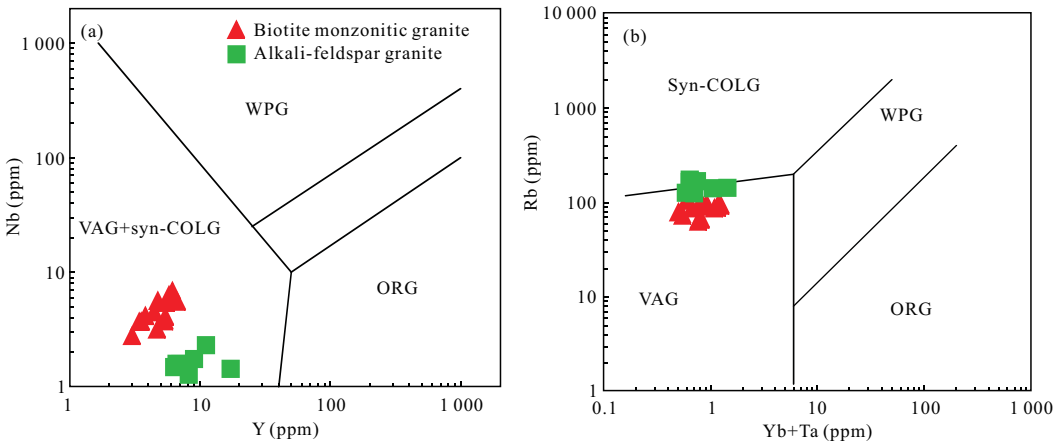


Figure 11. (a) Nb vs. Y and (b) Rb vs. (Yb+Nb) diagrams of the biotite monzonitic granite and the alkali-feldspar granite from Huichizi complex (Pearce et al., 1984). Abbreviations are: syn-COLG. syn-collisional granites; VAG. volcanic arc granites; WPG. within-plate granites; ORG. ocean ridge granite.

et al., 2004; Zhang B R et al., 1996). The granites show the characteristics of continental granitoids can be considered as products of the collision between the NCB and Qinling microcontinent. The conversion time of the collision, from extrusion to extension, in the NQB Caledonian was ~430 Ma.

The collision between the NCB and Qinling microcontinental thickened the crust, which heated and melted the juvenile basaltic lower crust and some of the ancient crust. This process formed the biotite monzonitic granites of the Huichizi complex. Following this event, crust extrusion obviously weakened at 430 Ma. Meanwhile, the activity and thickness of the crust decreased because of uplift and extension of the continental crust, leading to a more effective partial melting of the lower crust. The source environment changed from garnet phase equilibrium to plagioclase phase equilibrium, including more ancient crust, to produce alkali feldspar granites. Thereafter, the NQB entered a relatively stable post-collision evolution stage.

5 CONCLUSIONS

(1) The U-Pb zircon ages indicate that the Huichizi granitic complex is the product of multi-periodic magmatism. The biotite monzonitic granites intruded at 437 Ma and alkali-feldspar granites intruded at 424 Ma.

(2) The major and trace elements of the granites show the characteristics of adakitic rocks, indicating that the granites were derived from the partial melting of a thickened basaltic lower crust. Moreover, it is concluded that monzonitic granites were derived under a pressure of above 2.0 GPa (>60 km) and alkali-feldspar granites were derived under a pressure of 1.5 GPa (<50 km).

(3) Both granites possess similar source characteristics, which are also similar to Songshugou mafic-ultramafic ophiolites. The granites were derived from the basaltic lower continental crust accreted from the depleted mantle during the Neo-Mesoproterozoic Period. It is also indicated that the continental crustal growth occurred during the Neo-Mesoproterozoic Period.

(4) The Huichizi complex witnessed the process of extrusion stage to extension because of the collision between the NCB and Qinling microcontinent. The conversion time of the collision, from extrusion to extension, in the NQB Caledonian is ~430 Ma.

ACKNOWLEDGMENTS

This research was financially supported by the National Basic Research Program of China (No. 2014CB440906), the Strategic Priority Research Program (B) of Chinese Academy of Sciences (No. XDB18030200), and the National Natural Sciences Foundation of China (Nos. 41473049, 41103027). The authors are grateful to Dr. Zhaochu Hu from China University of Geosciences and Dr. Tao Yang from Nanjing University for their great help with expert isotopic analysis support. We appreciate two anonymous reviewers, who improved the paper greatly. The final publication is available at Springer via <https://doi.org/10.1007/s12583-017-0906-6>.

Electronic Supplementary Materials: Supplementary materials (Tables S1–S4) are available in the online version of this article at <https://doi.org/10.1007/s12583-017-0906-6>.

REFERENCES CITED

- Amelin, Y., Lee, D. C., Halliday, A. N., et al., 1999. Nature of the Earth's Earliest Crust from Hafnium Isotopes in Single Detrital Zircons. *Nature*, 399(6733): 252–255. <https://doi.org/10.1038/20426>
- Bader, T., Ratschbacher, L., Franz, L., et al., 2013. The Heart of China Revisited, I. Proterozoic Tectonics of the Qin Mountains in the Core of Supercontinent Rodinia. *Tectonics*, 32(3): 661–687. <https://doi.org/10.1002/tect.20024>
- Beard, J. S., Lofgren, G. E., 1991. Dehydration Melting and Water-Saturated Melting of Basaltic and Andesitic Greenstones and Amphibolites at 1, 3, and 6.9 kb. *Journal of Petrology*, 32(2): 365–401. <https://doi.org/10.1093/petrology/32.2.365>
- Belousova, E., Griffin, W., O'Reilly, S. Y., et al., 2002. Igneous Zircon: Trace Element Composition as an Indicator of Source Rock Type. *Contributions to Mineralogy and Petrology*, 143(5): 602–622. <https://doi.org/10.1007/s00410-002-0364-7>
- Blichert-Toft, J., Albarède, F., 1997. The Lu-Hf Isotope Geochemistry of Chondrites and the Evolution of the Mantle-Crust System. *Earth and Planetary Science Letters*, 148(1/2): 243–258. [https://doi.org/10.1016/s0012-821x\(97\)00040-x](https://doi.org/10.1016/s0012-821x(97)00040-x)
- Bottazzi, P., Tiepolo, M., Vannucci, R., et al., 1999. Distinct Site Preferences for Heavy and Light REE in Amphibole and the Prediction of Amph/LD REE. *Contributions to Mineralogy and Petrology*, 137(1/2): 36–45. <https://doi.org/10.1007/s004100050580>

- Cao, Y., Song, S. G., Su, L., et al., 2016. Highly Refractory Peridotites in Songshugou, Qinling Orogen: Insights into Partial Melting and Melt/Fluid-Rock Reactions in Forearc Mantle. *Lithos*, 252/253: 234–254. <https://doi.org/10.13039/501100001809>
- Castillo, P. R., 2006. An Overview of Adakite Petrogenesis. *Chinese Science Bulletin*, 51(3): 257–268. <https://doi.org/10.1007/s11434-006-0257-7>
- Castillo, P. R., Janney, P. E., Solidum, R. U., 1999. Petrology and Geochemistry of Camiguin Island, Southern Philippines: Insights to the Source of Adakites and Other Lavas in a Complex Arc Setting. *Contributions to Mineralogy and Petrology*, 134(1): 33–51. <https://doi.org/10.1007/s004100050467>
- Chen, D. L., 2004. LA-ICP-MS Zircon U-Pb Dating for High-Pressure Basic Granulite from North Qinling and Its Geological Significance. *Chinese Science Bulletin*, 49(21): 2296–2304 (in Chinese)
- Chen, D. L., Liu, L., 2011. New Data on the Chronology of Eclogite Andassociated Rock from Guanpo Area, North Qinling Orogeny and Its Constraint on Nature of North Qinling HP-UHP Eclogite Terrane. *Earth Science Frontiers*, 18(2): 158–168 (in Chinese with English abstract)
- Chen, D. L., Ren, Y. F., Gong, X. K., et al., 2015. Identification and Its Geological Significance of Eclogite Insongshugou, the North Qinling. *Acta Petrologica Sinica*, 31(7): 1841–1854 (in Chinese with English Abstract)
- Chen, N. S., Han, Y. Q., You, Z. D., et al., 1991. Whole-Rock Sm-Nd, Rb-Sr, and Single Grain Zircon Pb-Pb Dating of Complex Rocks from the Interior of the Qinling Orogenic Belt, Western Henan and Its Crustal Evolution. *Geochemica*, 20(3): 219–228 (in Chinese with English Abstract)
- Chen, Y. J., 2010. Indosinian Tectonic Setting, Magmatism and Metallogenesis in Qinling Orogen, Central China. *Geology in China*, 37(4): 854–866 (in Chinese with English Abstract)
- Cheng, H., Zhang, C., Vervoort, J. D., et al., 2011. Geochronology of the Transition of Eclogite to Amphibolite Facies Metamorphism in the North Qinling Orogen of Central China. *Lithos*, 125(3/4): 969–983. <https://doi.org/10.1016/j.lithos.2011.05.010>
- Cheng, H., Zhang, C., Vervoort, J. D., et al., 2012. Timing of Eclogite Facies Metamorphism in the North Qinling by U-Pb and Lu-Hf Geochronology. *Lithos*, 136–139: 46–59. <https://doi.org/10.1016/j.lithos.2011.06.003>
- Chung, S. L., Liu, D. Y., Ji, J. Q., et al., 2003. Adakites from Continental Collision Zones: Melting of Thickened Lower Crust beneath Southern Tibet. *Geology*, 31(11): 1021. <https://doi.org/10.1130/g19796.1>
- Defant, M. J., Drummond, M. S., 1990. Derivation of Some Modern Arc Magmas by Melting of Young Subducted Lithosphere. *Nature*, 347(6294): 662–665. <https://doi.org/10.1038/347662a0>
- Ding, X., Hu, Y. H., Zhang, H., et al., 2013. Major Nb/Ta Fractionation Recorded in Garnet Amphibolite Facies Metagabbro. *The Journal of Geology*, 121(3): 255–274. <https://doi.org/10.1086/669978>
- Ding, X., Lundstrom, C., Huang, F., et al., 2009. Natural and Experimental Constraints on Formation of the Continental Crust Based on Niobium-Tantalum Fractionation. *International Geology Review*, 51(6): 473–501. <https://doi.org/10.1080/00206810902759749>
- Diwu, C. R., Sun, Y., Liu, L., et al., 2010. The Disintegration of Kuanping Group in North Qinling Orogenic Belts and Neo-Proterozoic N-MORB. *Acta Petrologica Sinica*, 26(7): 2025–2038 (in Chinese with English Abstract)
- Diwu, C. R., Sun, Y., Zhao, Y., et al., 2014. Geochronological, Geochemical, and Nd-Hf Isotopic Studies of the Qinling Complex, Central China: Implications for the Evolutionary History of the North Qinling Orogenic Belt. *Geoscience Frontiers*, 5(4): 499–513. <https://doi.org/10.1016/j.gsf.2014.04.001>
- Dong, Y. P., Genser, J., Neubauer, F., et al., 2011a. U-Pb and $^{40}\text{Ar}/^{39}\text{Ar}$ Geochronological Constraints on the Exhumation History of the North Qinling Terrane, China. *Gondwana Research*, 19(4): 881–893. <https://doi.org/10.1016/j.gr.2010.09.007>
- Dong, Y. P., Zhang, G. W., Hauzenberger, C., et al., 2011b. Palaeozoic Tectonics and Evolutionary History of the Qinling Orogen: Evidence from Geochemistry and Geochronology of Ophiolite and Related Volcanic Rocks. *Lithos*, 122(1/2): 39–56. <https://doi.org/10.13039/501100001809>
- Dong, Y. P., Zhang, G. W., Neubauer, F., et al., 2011c. Tectonic Evolution of the Qinling Orogen, China: Review and Synthesis. *Journal of Asian Earth Sciences*, 41(3): 213–237. <https://doi.org/10.1016/j.jseas.2011.03.002>
- Dong, Y. P., Santosh, M., 2016. Tectonic Architecture and Multiple Orogeny of the Qinling Orogenic Belt, Central China. *Gondwana Research*, 29(1): 1–40. <https://doi.org/10.13039/501100001809>
- Dong, Y. P., Yang, Z., Liu, X. M., et al., 2014. Neoproterozoic Amalgamation of the Northern Qinling Terrain to the North China Craton: Constraints from Geochronology and Geochemistry of the Kuanping Ophiolite. *Precambrian Research*, 255: 77–95. <https://doi.org/10.13039/501100001809>
- Dong, Y. P., Zhang, X. N., Liu, X. M., et al., 2015. Propagation Tectonics and Multiple Accretionary Processes of the Qinling Orogen. *Journal of Asian Earth Sciences*, 104: 84–98. <https://doi.org/10.13039/501100001809>
- Dostal, J., Chatterjee, A. K., 2000. Contrasting Behaviour of Nb/Ta and Zr/Hf Ratios in a Peraluminous Granitic Pluton (Nova Scotia, Canada). *Chemical Geology*, 163(1–4): 207–218. [https://doi.org/10.1016/s0009-2541\(99\)00113-8](https://doi.org/10.1016/s0009-2541(99)00113-8)
- Feeley, T. C., Hacker, M. D., 1995. Intracrustal Derivation of Na-Rich Andesitic and Dacitic Magmas: An Example from Volcán Ollagüe, Andean Central Volcanic Zone. *The Journal of Geology*, 103(2): 213–225. <https://doi.org/10.1086/629737>
- Foley, S. F., Barth, M. G., Jenner, G. A., 2000. Rutile/Melt Partition Coefficients for Trace Elements and an Assessment of the Influence of Rutile on the Trace Element Characteristics of Subduction Zone Magmas. *Geochimica et Cosmochimica Acta*, 64(5): 933–938. [https://doi.org/10.1016/s0016-7037\(99\)00355-5](https://doi.org/10.1016/s0016-7037(99)00355-5)
- Foley, S., Tiepolo, M., Vannucci, R., 2002. Growth of Early Continental Crust Controlled by Melting of Amphibolite in Subduction Zones. *Nature*, 417(6891): 837–840. <https://doi.org/10.1038/nature00799>
- Gao, S., Rudnick, R. L., Yuan, H. L., et al., 2004. Recycling Lower Continental Crust in the North China Craton. *Nature*, 432(7019): 892–897. <https://doi.org/10.1038/nature03162>
- Green, T. H., 1995. Significance of Nb/Ta as an Indicator of Geochemical Processes in the Crust-Mantle System. *Chemical Geology*, 120(3/4): 347–359. [https://doi.org/10.1016/0009-2541\(94\)00145-x](https://doi.org/10.1016/0009-2541(94)00145-x)
- Griffin, W. L., Wang, X., Jackson, S. E., et al., 2002. Zircon Chemistry and Magma Mixing, SE China: In-Situ Analysis of Hf Isotopes, Tonglu and Pingtan Igneous Complexes. *Lithos*, 61(3/4): 237–269. [https://doi.org/10.1016/s0024-4937\(02\)00082-8](https://doi.org/10.1016/s0024-4937(02)00082-8)
- Guo, F., Nakamura, E., Fan, W., et al., 2007. Generation of Palaeocene Adakitic Andesites by Magma Mixing, Yanji Area, NE China. *Journal of Petrology*, 48(4): 661–692. <https://doi.org/10.1093/petrology/egl077>
- Hacker, B. R., Ratschbacher, L., Liou, J. G., 2004. Subduction, Collision and Exhumation in the Ultrahigh-Pressure Qinling-Dabie Orogen. *Geological Society, London, Special Publications*, 226(1): 157–175. <https://doi.org/10.1144/gsl.sp.2004.226.01.09>
- Hoskin, P. W. O., Black, L. P., 2002. Metamorphic Zircon Formation by Solid-State Recrystallization of Protolith Igneous Zircon. *Journal of Metamorphic Geology*, 18(4): 423–439. <https://doi.org/10.1046/j.1525-1314.2000.00266.x>
- Hu, J. M., Cui, J. T., Meng, Q. R., et al., 2004. The U-Pb Age of Zircons Sepa-

- rated from the Zhashui Granite in Qinling Orogen and Its Significance. *Geological Review*, 50(3): 323–329 (in Chinese with English Abstract)
- Huang, F., He, Y. S., 2010. Partial Melting of the Dry Mafic Continental Crust: Implications for Petrogenesis of C-Type Adakites. *Chinese Science Bulletin*, 55(22): 2428–2439. <https://doi.org/10.1007/s11434-010-3224-2>
- Huang, X. L., Xu, Y. G., Lan, J. B., et al., 2009. Neoproterozoic Adakitic Rocks from Mopanshan in the Western Yangtze Craton: Partial Melts of a Thickened Lower Crust. *Lithos*, 112(3/4): 367–381. <https://doi.org/10.1016/j.lithos.2009.03.028>
- Jochum, K. P., Seufert, H. M., Spettel, B., et al., 1986. The Solar-System Abundances of Nb, Ta, and Y, and the Relative Abundances of Refractory Lithophile Elements in Differentiated Planetary Bodies. *Geochimica et Cosmochimica Acta*, 50(6): 1173–1183. [https://doi.org/10.1016/0016-7037\(86\)90400-x](https://doi.org/10.1016/0016-7037(86)90400-x)
- Kay, R. W., Kay, S. M., 2002. Andean Adakites: Three Ways to Make them. *Acta Petrologica Sinica*, 18(2): 303–311 (in Chinese with English Abstract)
- Kröner, A., Zhang, G. W., Sun, Y., 1993. Granulites in the Tongbai Area, Qinling Belt, China: Geochemistry, Petrology, Single Zircon Geochronology, and Implications for the Tectonic Evolution of Eastern Asia. *Tectonics*, 12(1): 245–255. <https://doi.org/10.1029/92tc01788>
- Lei, M., 2010. Petrogenesis of Granites and Their Relation to Tectonic Evolution of Orogen in the East Part of Qinling Orogenic Belt: [Dissertation]. Chinese Academy of Geological Sciences, Beijing. 1–162 (in Chinese)
- Li, N., Chen, Y. J., Santosh, M., et al., 2015. Compositional Polarity of Triassic Granitoids in the Qinling Orogen, China: Implication for Termination of the Northernmost Paleo-Tethys. *Gondwana Research*, 27(1): 244–257. <https://doi.org/10.13039/501100001809>
- Li, S. Z., Kusky, T. M., Wang, L., et al., 2007. Collision Leading to Multiple-Stage Large-Scale Extrusion in the Qinling Orogen: Insights from the Mianlue Suture. *Gondwana Research*, 12(1/2): 121–143. <https://doi.org/10.1016/j.gr.2006.11.011>
- Li, W., Wang, T., Wang, X., 2001. Source of Huchizi Granitoid Complex Pluton in Northern Qinling, Central China: Constrained in Element and Isotopic Geochemistry. *Earth Science—Journal of China University of Geosciences*, 26(3): 269–278 (in Chinese with English Abstract)
- Li, W., Wang, T., Wang, X., et al., 2000. Single Zircon Dating of the Huichizi Complex, North Qinling: Its Geological Significance. *Regional Geology of China*, 19(2): 172–174 (in Chinese with English Abstract)
- Liang, J. L., Ding, X., Sun, X. M., et al., 2009. Nb/Ta Fractionation Observed in Eclogites from the Chinese Continental Scientific Drilling Project. *Chemical Geology*, 268(1/2): 27–40. <https://doi.org/10.1016/j.chemgeo.2009.07.006>
- Liu, B. X., 2014. Magmatism and Crustal Evolution in the Eastern North Qinling Terrain: [Dissertation]. University of Science and Technology of China, Hefei. 90–162 (in Chinese with English Abstract)
- Liu, J. F., Sun, Y., Tong, L. X., et al., 2009. Emplacement Age of the Songshugou Ultramafic Massif in the Qinling Orogenic Belt, and Geologic Implications. *International Geology Review*, 51(1): 58–76. <https://doi.org/10.1080/00206810802650576>
- Liu, L., Chen, D. L., Sun, Y., et al., 2003. Discovery of Relic Majoritic Garnet in Felsic Metamorphic Rocks of Qinling Complex, North Qinling Orogenic Belt, China. Alice Wain Memorial Western Norway Eclogite Field Symposium, Selje, Western Norway. 1: 82
- Liu, L., Liao, X. Y., Zhang, C. L., et al., 2013. Multi-Metamorphic Timings of HP-UHP Rocks in the North Qinling and Their Geological Implications. *Acta Petrologica Sinica*, 29(5): 1634–1656 (in Chinese with English Abstract)
- Liu, L., Yang, J. X., Chen, D. L., et al., 2010. Progress and Controversy in the Study of HP-UHP Metamorphic Terranes in the West and Middle Central China Orogen. *Journal of Earth Science*, 21(5): 581–597. <https://doi.org/10.1007/s12583-010-0128-7>
- Liu, Q., Wu, Y. B., Wang, H., et al., 2014. Zircon U-Pb Ages and Hf Isotope Compositions of Migmatites from the North Qinling Terrane and Their Geological Implications. *Journal of Metamorphic Geology*, 32(2): 177–193. <https://doi.org/10.1111/jmg.12065>
- Liu, Y. S., Hu, Z. C., Gao, S., et al., 2008. In situ Analysis of Major and Trace Elements of Anhydrous Minerals by LA-ICP-MS without Applying an Internal Standard. *Chemical Geology*, 257(1/2): 34–43. <https://doi.org/10.1016/j.chemgeo.2008.08.004>
- Liu, Y. S., Hu, Z. C., Zong, K. Q., et al., 2010. Reappraisal and Refinement of Zircon U-Pb Isotope and Trace Element Analyses by LA-ICP-MS. *Chinese Science Bulletin*, 55(15): 1535–1546. <https://doi.org/10.1007/s11434-010-3052-4>
- Lu, S. N., Chen, Z. H., Xiang, Z. Q., 2006. U-Pb Ages of Detrital Zircons from the Para-Metamorphic Rocks of the Qinling Group and Their Geological Significance. *Earth Science Frontiers*, 13(6): 303–310 (in Chinese with English Abstract)
- Lu, S. N., Li, H. K., Chen, Z. H., et al., 2003. Neoproterozoic Geological Evolution of the Qinling Orogen and Respond to Events of Rodinia Supercontinents. Geology Publishing House, Beijing. 1–193 (in Chinese)
- Lu, S. N., Yu, H. F., Li, H. K., et al., 2009. Precambrian Geology of Central Orogen (Western and Middle Part). Geology Publishing House, Beijing. 203 (in Chinese)
- Lu, X. X., Dong, Y., Chang, Q. L., et al., 1996. Indosinian Shahewan Rappaki Granite in Qinling and Its Dynamic Significance. *Science in China(Series D: Earth Sciences)*, 39(3): 266–272 (in Chinese)
- Lu, X. X., Dong, Y., Wei, X. D., et al., 1999. Age of Tuwushan A-Type Granite in the East Qinling and Its Tectonic Implications. *Chinese Science Bulletin*, 44(9): 975–978 (in Chinese with English Abstract)
- Ludwig, K. R., 2003. User's Manual for Isoplot 3.00. A Geochronological Toolkit for Microsoft Excel. Berkeley Geochronology Center, CA Special Publication, Berkeley. 1–10
- Ma, L., Wang, B. D., Jiang, Z. Q., et al., 2014. Petrogenesis of the Early Eocene Adakitic Rocks in the Napuri Area, Southern Lhasa: Partial Melting of Thickened Lower Crust during Slab Break-off and Implications for Crustal Thickening in Southern Tibet. *Lithos*, 196/197: 321–338. <https://doi.org/10.1016/j.lithos.2014.02.011>
- Macpherson, C. G., Dreher, S. T., Thirlwall, M. F., 2006. Adakites without Slab Melting: High Pressure Differentiation of Island Arc Magma, Mindanao, the Philippines. *Earth and Planetary Science Letters*, 243(3/4): 581–593. <https://doi.org/10.1016/j.epsl.2005.12.034>
- Maniar, P. D., Piccoli, P. M., 1989. Tectonic Discrimination of Granitoids. *Geological Society of America Bulletin*, 101(5): 635–643. [https://doi.org/10.1130/0016-7606\(1989\)101<0635:tdog>2.3.co;2](https://doi.org/10.1130/0016-7606(1989)101<0635:tdog>2.3.co;2)
- Martin, H., 1999. Adakitic Magmas: Modern Analogues of Archaean Granitoids. *Lithos*, 46(3): 411–429. [https://doi.org/10.1016/s0024-4937\(98\)00076-0](https://doi.org/10.1016/s0024-4937(98)00076-0)
- Martin, H., Smithies, R. H., Rapp, R., et al., 2005. An Overview of Adakite, Tonalite-Trondhjemite-Granodiorite (TTG), and Sanukitoid: Relationships and Some Implications for Crustal Evolution. *Lithos*, 79(1/2): 1–24. <https://doi.org/10.1016/j.lithos.2004.04.048>
- Mattauer, M., Matte, P., Malavieille, J., et al., 1985. Tectonics of the Qinling Belt: Build-up and Evolution of Eastern Asia. *Nature*, 317(6037): 496–500. <https://doi.org/10.1038/317496a0>
- Meng, Q. R., Zhang, G. W., 1999. Timing of Collision of the North and South

- China Blocks: Controversy and Reconciliation. *Geology*, 27(2): 123. [https://doi.org/10.1130/0091-7613\(1999\)027<0123:tocotn>2.3.co;2](https://doi.org/10.1130/0091-7613(1999)027<0123:tocotn>2.3.co;2)
- Meng, Q. R., Zhang, G. W., 2000. Geologic Framework and Tectonic Evolution of the Qinling Orogen, Central China. *Tectonophysics*, 323(3/4): 183–196. [https://doi.org/10.1016/s0040-1951\(00\)00106-2](https://doi.org/10.1016/s0040-1951(00)00106-2)
- Middlemost, E. A. K., 1994. Naming Materials in the Magma/Igneous Rock System. *Earth-Science Reviews*, 37(3/4): 215–224. [https://doi.org/10.1016/0012-8252\(94\)90029-9](https://doi.org/10.1016/0012-8252(94)90029-9)
- Moyen, J. F., 2009. High Sr/Y and La/Yb Ratios: The Meaning of the “Adakitic Signature”. *Lithos*, 112(3/4): 556–574. <https://doi.org/10.1016/j.lithos.2009.04.001>
- Muir, R. J., Weaver, S. D., Bradshaw, J. D., et al., 1995. The Cretaceous Separation Point Batholith, New Zealand: Granitoid Magmas Formed by Melting of Mafic Lithosphere. *Journal of the Geological Society*, 152(4): 689–701. <https://doi.org/10.1144/gsjgs.152.4.0689>
- Peacock, S. M., Rushmer, T., Thompson, A. B., 1994. Partial Melting of Subducting Oceanic Crust. *Earth and Planetary Science Letters*, 121(1/2): 227–244. [https://doi.org/10.1016/0012-821x\(94\)90042-6](https://doi.org/10.1016/0012-821x(94)90042-6)
- Pearce, J. A., Harris, N. B. W., Tindle, A. G., 1984. Trace Element Discrimination Diagrams for the Tectonic Interpretation of Granitic Rocks. *Journal of Petrology*, 25(4): 956–983. <https://doi.org/10.1093/petrology/25.4.956>
- Petford, N., Atherton, M., 1996. Na-Rich Partial Melts from Newly Underplated Basaltic Crust: The Cordillera Blanca Batholith, Peru. *Journal of Petrology*, 37(6): 1491–1521. <https://doi.org/10.1093/petrology/37.6.1491>
- Prouteau, G., Scaillet, B., Pichavant, M., et al., 2001. Evidence for Mantle Metasomatism by Hydrous Silicic Melts Derived from Subducted Oceanic Crust. *Nature*, 410(6825): 197–200. <https://doi.org/10.1038/35065583>
- Qi, L., Hu, J., Gregoire, D. C., 2000. Determination of Trace Elements in Granites by Inductively Coupled Plasma Mass Spectrometry. *Talanta*, 51(3): 507–513. [https://doi.org/10.1016/S0039-9140\(99\)00318-5](https://doi.org/10.1016/S0039-9140(99)00318-5)
- Qian, J. H., Yang, X. Q., Liu, L., et al., 2013. Zircon U-Pb Dating, Mineral Inclusions, Lu-Hf Isotopic Data and Their Geological Significance of Garnet Amphibolite from Songshugou, North Qinling. *Acta Petrologica Sinica*, 29(9): 3087–3098 (in Chinese with English Abstract)
- Qian, Q., Hermann, J., 2013. Partial Melting of Lower Crust at 10–15 kbar: Constraints on Adakite and TTG Formation. *Contributions to Mineralogy and Petrology*, 165(6): 1195–1224. <https://doi.org/10.1007/s00410-013-0854-9>
- Qin, J. F., 2010. Petrogenesis and Geodynamic Implications of the Late-Triassic Granitoids from the Qinling Orogenic Belt [Dissertation]. Northwest University, Xi'an. 78–163 (in Chinese with English Abstract)
- Qin, J. F., Lai, S. C., Li, Y. F., 2007. Genesis of the Indosinian Guangtoushan Adakitic Biotite Plagiogranite in the Mianxian-Lueyang (Mianlue) Suture, South Qinling, China, and Its Tectonic Implications. *Geological Bulletin of China*, 26(4): 466–471 (in Chinese with English Abstract)
- Qin, J. F., Lai, S. C., Li, Y. F., 2013. Multi-Stage Granitic Magmatism during Exhumation of Subducted Continental Lithosphere: Evidence from the Wulong Pluton, South Qinling. *Gondwana Research*, 24(3/4): 1108–1126. <https://doi.org/10.1016/j.gr.2013.02.005>
- Qin, Z. W., Wu, Y. B., Siebel, W., et al., 2015. Genesis of Adakitic Granitoids by Partial Melting of Thickened Lower Crust and Its Implications for Early Crustal Growth: A Case Study from the Huichizi Pluton, Qinling Orogen, Central China. *Lithos*, 238: 1–12. <https://doi.org/10.13039/501100001809>
- Rapp, R. P., Shimizu, N., Norman, M. D., et al., 1999. Reaction between Slab-Derived Melts and Peridotite in the Mantle Wedge: Experimental Constraints at 3.8 GPa. *Chemical Geology*, 160(4): 335–356. [https://doi.org/10.1016/s0009-2541\(99\)00106-0](https://doi.org/10.1016/s0009-2541(99)00106-0)
- Rapp, R. P., Watson, E. B., 1995. Dehydration Melting of Metabasalt at 8–32 kbar: Implications for Continental Growth and Crust-Mantle Recycling. *Journal of Petrology*, 36(4): 891–931. <https://doi.org/10.1093/petrology/36.4.891>
- Rapp, R. P., Watson, E. B., Miller, C. F., 1991. Partial Melting of Amphibolite/Eclogite and the Origin of Archean Trondhjemites and Tonalites. *Precambrian Research*, 51(1–4): 1–25. [https://doi.org/10.1016/0301-9268\(91\)90092-o](https://doi.org/10.1016/0301-9268(91)90092-o)
- Ratschbacher, L., Hacker, B. R., Calvert, A., et al., 2003. Tectonics of the Qinling (Central China): Tectonostratigraphy, Geochronology, and Deformation History. *Tectonophysics*, 366(1/2): 1–53. [https://doi.org/10.1016/s0040-1951\(03\)00053-2](https://doi.org/10.1016/s0040-1951(03)00053-2)
- Ren, J. S., Niu, B. G., Liu, Z. G., 1999. Soft Collision, Superposition Orogeny and Polycyclic Suturing. *Earth Science Frontiers*, 6(3): 85–93 (in Chinese with English Abstract)
- Rudnick, R. L., Gao, S., 2003. Composition of the Continental Crust. *Treatise on Geochemistry*, 3: 1–64
- Rushmer, T., 1991. Partial Melting of Two Amphibolites: Contrasting Experimental Results under Fluid-Absent Conditions. *Contributions to Mineralogy and Petrology*, 107(1): 41–59. <https://doi.org/10.1007/bf00311184>
- Scherer, E., 2001. Calibration of the Lutetium-Hafnium Clock. *Science*, 293(5530): 683–687. <https://doi.org/10.1126/science.1061372>
- Sen, C., Dunn, T., 1994. Dehydration Melting of a Basaltic Composition Amphibolite at 1.5 and 2.0 GPa: Implications for the Origin of Adakites. *Contributions to Mineralogy and Petrology*, 117(4): 394–409. <https://doi.org/10.1007/bf00307273>
- Shi, Y., Yu, J. H., Santosh, M., 2013. Tectonic Evolution of the Qinling Orogenic Belt, Central China: New Evidence from Geochemical, Zircon U-Pb Geochronology and Hf Isotopes. *Precambrian Research*, 231(5): 19–60. <https://doi.org/10.1016/j.precamres.2013.03.001>
- Shi, Y., Yu, J. H., Xu, X. S., et al., 2009. Geochronology and Geochemistry of the Qinling Group in the Eastern Qinling Orogen. *Acta Petrologica Sinica*, 25(10): 2651–2670 (in Chinese with English Abstract)
- Smithies, R. H., 2000. The Archaean Tonalite-Trondhjemite-Granodiorite (TTG) Series is not an Analogue of Cenozoic Adakite. *Earth and Planetary Science Letters*, 182(1): 115–125. [https://doi.org/10.1016/s0012-821x\(00\)00236-3](https://doi.org/10.1016/s0012-821x(00)00236-3)
- Stern, C. R., Kilian, R., 1996. Role of the Subducted Slab, Mantle Wedge and Continental Crust in the Generation of Adakites from the Andean Austral Volcanic Zone. *Contributions to Mineralogy and Petrology*, 123(3): 263–281. <https://doi.org/10.1007/s004100050155>
- Streck, M. J., Leeman, W. P., Chesley, J., 2007. High-Magnesian Andesite from Mount Shasta: A Product of Magma Mixing and Contamination, not a Primitive Mantle Melt. *Geology*, 35(4): 351. <https://doi.org/10.1130/g23286a.1>
- Sun, S. S., McDonough, W. F., 1989. Chemical and Isotopic Systematics of Oceanic Basalts: Implications for Mantle Composition and Processes. *Geological Society, London, Special Publications*, 42(1): 313–345. <https://doi.org/10.1144/gsl.sp.1989.042.01.19>
- Sun, W. D., Li, S. G., Chen, Y. D., et al., 2002. Timing of Synorogenic Granitoids in the South Qinling, Central China: Constraints on the Evolution of the Qinling-Dabie Orogenic Belt. *The Journal of Geology*, 110(4): 457–468. <https://doi.org/10.1086/340632>
- Sun, Y., Lu, X., Han, S., et al., 1996. Composition and Formation of Paleozoic Erlangping Ophiolitic Slab, North Qinling: Evidence from Geology and Geochemistry. *Science in China Series D: Earth Sciences*, 39(SI): 50–59
- Sun, W. D., Li, S. G., Sun, Y., et al., 1996. Chronology and Geochemistry of a Lava Pillow in the Erlangping Group at Xixia in the Northern Qinling Mountains. *Geological Review*, 42(6): 144–153 (in Chinese with English Abstract)

- lish Abstract)
- Vervoort, J. D., Blichert-Toft, J., 1999. Evolution of the Depleted Mantle: Hf Isotope Evidence from Juvenile Rocks through Time. *Geochimica et Cosmochimica Acta*, 63(3/4): 533–556. [https://doi.org/10.1016/s0016-7037\(98\)00274-9](https://doi.org/10.1016/s0016-7037(98)00274-9)
- Vervoort, J. D., Patchett, P. J., 1996. Behavior of Hafnium and Neodymium Isotopes in the Crust: Constraints from Precambrian Crustally Derived Granites. *Geochimica et Cosmochimica Acta*, 60(19): 3717–3733. [https://doi.org/10.1016/0016-7037\(96\)00201-3](https://doi.org/10.1016/0016-7037(96)00201-3)
- Wan, Y. S., Liu, D. Y., Dong, C. Y., et al., 2011. SHRIMP Zircon Dating of Meta-Sedimentary Rock from the Qinling Group in the North of Xixia, North Qinling Orogenic Belt: Constraints on Complex Histories of Source Region and Timing of Deposition and Metamorphism. *Acta Petrologica Sinica*, 27(4): 1172–1178 (in Chinese with English Abstract)
- Wang, H., Wu, Y. B., Gao, S., et al., 2011. Eclogite Origin and Timings in the North Qinling Terrane, and Their Bearing on the Amalgamation of the South and North China Blocks. *Journal of Metamorphic Geology*, 29(9): 1019–1031. <https://doi.org/10.1111/j.1525-1314.2011.00955.x>
- Wang, H., Wu, Y. B., Gao, S., et al., 2013. Continental Origin of Eclogites in the North Qinling Terrane and Its Tectonic Implications. *Precambrian Research*, 230: 13–30. <https://doi.org/10.1016/j.precamres.2012.12.010>
- Wang, H., Wu, Y. B., Gao, S., et al., 2014a. Deep Subduction of Continental Crust in Accretionary Orogen: Evidence from U-Pb Dating on Diamond-Bearing Zircons from the Qinling Orogen, Central China. *Lithos*, 190/191(3): 420–429. <https://doi.org/10.1016/j.lithos.2013.12.021>
- Wang, H., Wu, Y. B., Li, C. R., et al., 2014b. Recycling of Sediment into the Mantle Source of K-Rich Mafic Rocks: Sr-Nd-Hf-O Isotopic Evidence from the Fushui Complex in the Qinling Orogen. *Contributions to Mineralogy and Petrology*, 168(4): 1–19. <https://doi.org/10.1007/s00410-014-1062-y>
- Wang, H., Wu, Y. B., Gao, S., et al., 2016. Continental Growth through Accreted Oceanic Arc: Zircon Hf-O Isotope Evidence for Granitoids from the Qinling Orogen. *Geochimica et Cosmochimica Acta*, 182: 109–130. <https://doi.org/10.13039/501100001809>
- Wang, Q., Wyman, D. A., Xu, J. F., et al., 2006. Petrogenesis of Cretaceous Adakitic and Shoshonitic Igneous Rocks in the Luzong Area, Anhui Province (Eastern China): Implications for Geodynamics and Cu-Au Mineralization. *Lithos*, 89(3/4): 424–446. <https://doi.org/10.1016/j.lithos.2005.12.010>
- Wang, Q., Wyman, D. A., Xu, J. F., et al., 2007. Partial Melting of Thickened or Delaminated Lower Crust in the Middle of Eastern China: Implications for Cu-Au Mineralization. *The Journal of Geology*, 115(2): 149–161. <https://doi.org/10.1086/510643>
- Wang, Q., Xu, J. F., Jian, P., et al., 2005. Petrogenesis of Adakitic Porphyries in an Extensional Tectonic Setting, Dexing, South China: Implications for the Genesis of Porphyry Copper Mineralization. *Journal of Petrology*, 47(1): 119–144. <https://doi.org/10.1093/petrology/egi070>
- Wang, T., Hu, N. G., Pei, X. Z., et al., 1997. The Composition, Tectonic Framework and Evolution of Qinling Complex, Central China. *Acta Geoscientia Sinica*, 18(4): 345–351 (in Chinese with English Abstract)
- Wang, T., Wang, X. X., Li, W. P., 2000. Evaluation of Multiple Emplacement Mechanisms: The Huichizi Granite Pluton, Qinling Orogenic Belt, Central China. *Journal of Structural Geology*, 22(4): 505–518. [https://doi.org/10.1016/s0191-8141\(99\)00169-8](https://doi.org/10.1016/s0191-8141(99)00169-8)
- Wang, T., Wang, X. X., Tian, W., et al., 2009. North Qinling Paleozoic Granite Associations and Their Variation in Space and Time: Implications for Orogenic Processes in the Orogens of Central China. *Science in China Series D: Earth Sciences*, 52(9): 1359–1384. <https://doi.org/10.1007/s11430-009-0129-5>
- Wang, X. X., Wang, T., Zhang, C. L., 2013. Neoproterozoic, Paleozoic, and Mesozoic Granitoid Magmatism in the Qinling Orogen, China: Constraints on Orogenic Process. *Journal of Asian Earth Sciences*, 72(4): 129–151. <https://doi.org/10.1016/j.jseas.2012.11.037>
- Wang, X. X., Wang, T., Zhang, C. L., 2015. Granitoid Magmatism in the Qinling Orogen, Central China and Its Bearing on Orogenic Evolution. *Science China: Earth Sciences*, 58(9): 1497–1512. <https://doi.org/10.1007/s11430-015-5150-2>
- Wareham, C. D., Millar, I. L., Vaughan, A. P. M., 1997. The Generation of Sodic Granite Magmas, Western Palmer Land, Antarctic Peninsula. *Contributions to Mineralogy and Petrology*, 128(1): 81–96. <https://doi.org/10.1007/s004100050295>
- Wiedenbeck, M., Allé, P., Corfu, F., et al., 1995. Three Natural Zircon Standards for U-Th-Pb, Lu-Hf, Trace Element and REE Analyses. *Geostandards and Geoanalytical Research*, 19(1): 1–23. <https://doi.org/10.1111/j.1751-908x.1995.tb00147.x>
- Wolde, B., Team, G. G. G., 1996. Tonalite-Trondhjemite-Granite Genesis by Partial Melting of Newly Underplated Basaltic Crust: An Example from the Neoproterozoic Birbir Magmatic Arc, Western Ethiopia. *Precambrian Research*, 76(1/2): 3–14. [https://doi.org/10.1016/0301-9268\(95\)00016-x](https://doi.org/10.1016/0301-9268(95)00016-x)
- Wolf, M. B., Wyllie, P. J., 1994. Dehydration-Melting of Amphibolite at 10 kbar: The Effects of Temperature and Time. *Contributions to Mineralogy and Petrology*, 115(4): 369–383. <https://doi.org/10.1007/bf00320972>
- Wu, F. Y., Li, X. H., Yang, J. H., et al., 2007. Discussions on the Petrogenesis of Granites. *Acta Petrologica Sinica*, 23(6): 1217–1238 (in Chinese with English Abstract)
- Wu, F. Y., Yang, Y. H., Xie, L. W., et al., 2006. Hf Isotopic Compositions of the Standard Zircons and Baddeleyites Used in U-Pb Geochronology. *Chemical Geology*, 234(1/2): 105–126. <https://doi.org/10.1016/j.chemgeo.2006.05.003>
- Wu, Y. B., Hanchar, J. M., Gao, S., et al., 2009. Age and Nature of Eclogites in the Huwan Shear Zone, and the Multi-Stage Evolution of the Qinling-Dabie-Sulu Orogen, Central China. *Earth and Planetary Science Letters*, 277(3/4): 345–354. <https://doi.org/10.1016/j.epsl.2008.10.031>
- Wu, Y. B., Zheng, Y. F., 2013. Tectonic Evolution of a Composite Collision Orogen: An Overview on the Qinling-Tongbai-Hong'an-Dabie-Sulu Orogenic Belt in Central China. *Gondwana Research*, 23(4): 1402–1428. <https://doi.org/10.13039/501100002855>
- Xiong, X. L., 2006. Trace Element Evidence for Growth of Early Continental Crust by Melting of Rutile-Bearing Hydrous Eclogite. *Geology*, 34(11): 945–948. <https://doi.org/10.1130/g22711a.1>
- Xiong, X. L., Adam, J., Green, T. H., 2005. Rutile Stability and Rutile/Melt HFSE Partitioning during Partial Melting of Hydrous Basalt: Implications for TTG Genesis. *Chemical Geology*, 218(3/4): 339–359. <https://doi.org/10.1016/j.chemgeo.2005.01.014>
- Xiong, X. L., Adam, J., Green, T. H., et al., 2006. Trace Element Characteristics of Partial Melts Produced by Melting of Metabasalts at High Pressures: Constraints on the Formation Condition of Adakitic Melts. *Science in China Series D: Earth Sciences*, 49(9): 915–925. <https://doi.org/10.1007/s11430-006-0915-2>
- Xiong, X. L., Keppler, H., Audétat, A., et al., 2011. Partitioning of Nb and Ta between Rutile and Felsic Melt and the Fractionation of Nb/Ta during Partial Melting of Hydrous Metabasalt. *Geochimica et Cosmochimica Acta*, 75(7): 1673–1692. <https://doi.org/10.1016/j.gca.2010.06.039>
- Xiong, X. L., Keppler, H., Audétat, A., et al., 2009. Experimental Constraints on Rutile Saturation during Partial Melting of Metabasalt at the Amphibolite to Eclogite Transition, with Applications to TTG Genesis. *American Journal of Mineralogy*, 24(1): 1–12. <https://doi.org/10.1007/s11430-008-0083-0>

- can *Mineralogist*, 94(8/9): 1175–1186.
<https://doi.org/10.2138/am.2009.3158>
- Xu, B., Grove, M., Wang, C. Q., et al., 2000. $^{40}\text{Ar}/^{39}\text{Ar}$ Thermochronology from the Northwestern Dabie Shan: Constraints on the Evolution of Qinling-Dabie Orogenic Belt, East-Central China. *Tectonophysics*, 322(3/4): 279–301. [https://doi.org/10.1016/s0040-1951\(00\)00092-5](https://doi.org/10.1016/s0040-1951(00)00092-5)
- Xue, F., Lerch, M. F., Kröner, A., et al., 1996. Tectonic Evolution of the East Qinling Mountains, China, in the Palaeozoic: A Review and New Tectonic Model. *Tectonophysics*, 253(3/4): 271–284. [https://doi.org/10.1016/0040-1951\(95\)00060-7](https://doi.org/10.1016/0040-1951(95)00060-7)
- Yan, Q. R., Wang, Z. Q., Yan, Z., et al., 2009. Tectonic Affinity and Timing of Two Types of Amphibolites within the Qinling Group, North Qinling Orogenic Belt. *Acta Petrologica Sinica*, 25(9): 2177–2194 (in Chinese with English Abstract)
- Yan, Z., Wang, Z. Q., Yan, Q. R., et al., 2006a. Devonian Sedimentary Environments and Provenance of the Qinling Orogen: Constraints on Late Paleozoic Southward Accretionary Tectonics of the North China Craton. *International Geology Review*, 48(7): 585–618. <https://doi.org/10.2747/0020-6814.48.7.585>
- Yan, Z., Wang, Z., Wang, T., et al., 2006b. Provenance and Tectonic Setting of Clastic Deposits in the Devonian Xicheng Basin, Qinling Orogen, Central China. *Journal of Sedimentary Research*, 76(3): 557–574. <https://doi.org/10.2110/jsr.2006.046>
- Yang, J. S., Liu, F. L., Wu, C., et al., 2005. Two Ultrahigh-Pressure Metamorphic Events Recognized in the Central Orogenic Belt of China: Evidence from the U-Pb Dating of Coesite-Bearing Zircons. *International Geology Review*, 47(4): 327–343. <https://doi.org/10.2747/0020-6814.47.4.327>
- Yang, J. S., Xu, Z. Q., Dobrzhinetskaya, L. F., et al., 2003. Discovery of Metamorphic Diamonds in Central China: An Indication of a >4 000-km-Long Zone of Deep Subduction Resulting from Multiple Continental Collisions. *Terra Nova*, 15(6): 370–379. <https://doi.org/10.1046/j.1365-3121.2003.00511.x>
- Yang, J. S., Xu, Z. Q., Pei, X. Z., et al., 2002. Discovery of Diamond in North Qinling: Evidence for a Giant UHPM Belt across Central China and Recognition of Paleozoic and Mesozoic Dual Deep Subduction between North China and Yangtze Plates. *Acta Geologica Sinica*, 76(4): 484–495 (in Chinese with English Abstract)
- Yang, L., Chen, F. K., Yang, Y. Z., et al., 2010. Zircon U-Pb Ages of the Qinling Group in Danfeng Area: Recording Mesoproterozoic and Neoproterozoic Magmatism and Early Paleozoic Metamorphism in the North Qinling Terrain. *Acta Petrologica Sinica*, 26(5): 1589–1603 (in Chinese with English Abstract)
- Yu, H., Zhang, H. F., Li, X. H., et al., 2016. Tectonic Evolution of the North Qinling Orogen from Subduction to Collision and Exhumation: Evidence from Zircons in Metamorphic Rocks of the Qinling Group. *Gondwana Research*, 30(1): 65–78. <https://doi.org/10.1016/j.gr.2015.07.003>
- Zhai, X. M., Day, H. W., Hacker, B. R., et al., 1998. Paleozoic Metamorphism in the Qinling Orogen, Tongbai Mountains, Central China. *Geology*, 26(4): 371. [https://doi.org/10.1130/0091-7613\(1998\)026<0371:pmitqo>2.3.co;2](https://doi.org/10.1130/0091-7613(1998)026<0371:pmitqo>2.3.co;2)
- Zhang, B. R., Zhang, H. F., Zhao, Z. D., et al., 1996. Geochemical Subdivision and Evolution of the Lithosphere in East Qinling and Adjacent Regions—Implications for Tectonics. *Science in China Series D: Earth Sciences*, 39(3): 245–255 (in Chinese with English Abstract)
- Zhang, C. L., Liu, L., Wang, T., et al., 2013. Granitic Magmatism Related to Early Paleozoic Continental Collision in North Qinling. *Chinese Science Bulletin*, 58(35): 4405–4410. <https://doi.org/10.1007/s11434-013-6064-z>
- Zhang, C. L., Liu, L., Zhang, G. W., et al., 2004. Determination of Neoproterozoic Post-Collisional Granites in the North Qinling Mountains and Its Tectonic Significance. *Earth Science Frontiers*, 11(3): 33–42 (in Chinese with English Abstract)
- Zhang, C. L., Zhang, G. W., Yan, Y. X., et al., 2005. Origin and Dynamic Significance of Guangtoushan Granitic Plutons to the North of Mianlue Zone in Southern Qinling. *Acta Petrologica Sinica*, 21(3): 711–720 (in Chinese with English Abstract)
- Zhang, G. B., Niu, Y. L., Song, S. G., et al., 2015. Trace Element Behavior and $P-T-t$ Evolution during Partial Melting of Exhumed Eclogite in the North Qaidam UHPM Belt (NW China): Implications for Adakite Genesis. *Lithos*, 226: 65–80. <https://doi.org/10.13039/501100001809>
- Zhang, G. W., 1988. Formation and Evolution of the Qinling Orogen. Northwest University Press, Xi'an. 1–192 (in Chinese with English Abstract)
- Zhang, G. W., Dong, Y. P., Lai, S. C., et al., 2004. Mianlue Tectonic Zone and Mianlue Suture Zone on Southern Margin of Qinling-Dabie Orogenic Belt. *Science in China Series D: Earth Sciences*, 47(4): 300–316. <https://doi.org/10.1360/02yd0526>
- Zhang, G. W., Meng, Q. R., Lai, S. C., 1995. Tectonics and Structure of the Qinling Orogenic Belt. *Science in China: Series B*, 11(38): 1379–1394 (in Chinese with English Abstract)
- Zhang, G. W., Meng, Q. R., Yu, Z. P., et al., 1996. Orogenesis and Dynamics of Qinling Orogen. *Science in China Series D: Earth Sciences*, 26(3): 193–200 (in Chinese with English Abstract)
- Zhang, G. W., Zhang, B. R., Yuan, X. C., et al., 2001. Qinling Orogenic Belt and Continental Dynamics. Science Press, Beijing (in Chinese with English Abstract)
- Zhang, H. F., Zhang, B. R., Luo, T. S., 1994. Discussion on the Source of the Materials of the Huichizi Granite Pluton in Northern Qinling Mountains, China. *Journal of Mineralogy and Petrology*, 14(1): 67–73 (in Chinese with English Abstract)
- Zhang, Z. Q., Liu, D. Y., Fu, G. M., 1994. Isotopic Geochronology of Metamorphic Strata in North Qinling. Geological Publishing House, Beijing (in Chinese with English Abstract)
- Zhang, Z. Q., Zhang, G. W., Liu, D. Y., et al., 2006. Isotopic Geochronology and Geochemistry of Ophiolites, Granites and Clasti Sedimentary Rocks in the Qinling-Dabie Orogenic Belt. Geological Publishing House, Beijing (in Chinese)
- Zhang, Z. Q., Zhang, G. W., Tang, S. H., et al., 1999. Age of the Shahewan Rapakivi Granite in the Qinling Orogen, China, and Its Constraints on the End Time of the Main Orogenic Stage of this Orogen. *Chinese Science Bulletin*, 44(21): 2001–2004. <https://doi.org/10.1007/bf02887128>
- Zheng, Y. F., Zhang, L. F., McClelland, W. C., et al., 2012. Processes in Continental Collision Zones: Preface. *Lithos*, 136–139(4): 1–9. <https://doi.org/10.1016/j.lithos.2011.11.020>
- Zhou, Z. J., Mao, S. D., Chen, Y. J., et al., 2016. U-Pb Ages and Lu-Hf Isotopes of Detrital Zircons from the Southern Qinling Orogen: Implications for Precambrian to Phanerozoic Tectonics in Central China. *Gondwana Research*, 35(4): 323–337. <https://doi.org/10.13039/501100001809>
- Zhu, X. Y., Chen, F. K., Li, S. Q., et al., 2011. Crustal Evolution of the North Qinling Terrain of the Qinling Orogen, China: Evidence from Detrital Zircon U-Pb Ages and Hf Isotopic Composition. *Gondwana Research*, 20(1): 194–204. <https://doi.org/10.1016/j.gr.2010.12.009>